Sinorhizobium meliloti functions required for resistance to antimicrobial NCR peptides and bacteroid differentiation

Quentin Nicoud[1,*], Quentin Barrière[1,*], Nicolas Busset[1,#,*], Sara Dendene[1], Dmitrii Travin[2,1], Mickaël Bourge[1], Romain Le Bars[1], Claire Boulogne[1], Marie Lecroël[1], Sándor Jenei[3], Atilla Kereszt[3], Eva Kondorosi[3], Emanuele G. Biondi[1], Tatiana Timchenko[1], Benoît Alunni[1], Peter Mergaert[1,#]

[1]Université Paris-Saclay, CEA, CNRS, Institute for Integrative Biology of the Cell (I2BC), Gif-sur-Yvette, France

[2]Center of Life Sciences, Skolkovo Institute of Science and Technology, Moscow, Russia

[3]Institute of Plant Biology, Biological Research Centre, Szeged, Hungary

*equal contribution

#present address: Plant Health Institute Montpellier, France

[#]correspondence: peter.mergaert@i2bc.paris-saclay.fr

Running title: NCR resistance in *Sinorhizobium meliloti*

Abstract

Legumes of the *Medicago* genus form symbiosis with the bacterium *Sinorhizobium meliloti* and develop root nodules housing large numbers of the intracellular symbionts. Members of the Nodule-specific Cysteine Rich peptide (NCRs) family induce the endosymbionts into a terminal differentiated state. Individual cationic NCRs are antimicrobial peptides that have the capacity to kill the symbiont but the nodule cell environment prevents killing. Moreover, the bacterial broad-specificity peptide uptake transporter BacA and exopolysaccharides contribute to protect the endosymbionts against the toxic activity of NCRs. Here, we show that other *S. meliloti* functions participate in the protection of the endosymbionts, including an additional broad-specificity peptide uptake transporter encoded by the *yejABEF* genes, lipopolysaccharide modifications mediated by *lpsB* and *lpxXL* as well as *rpoH1*, encoding a stress sigma factor. Mutants of these genes show *in vitro* a strain-specific increased sensitivity profile against a panel of NCRs and form nodules in which bacteroid differentiation is affected. The *lpsB* mutant nodule bacteria do not differentiate, the *lpxXL* and *rpoH1* mutants form some seemingly fully differentiated bacteroids although most of the nodule bacteria are undifferentiated, while the *yejABEF* mutants form hypertrophied but nitrogen-fixing bacteroids. The nodule bacteria of all the mutants have a strongly enhanced membrane permeability, which is dependent on the transport of NCRs to the endosymbionts. Our results suggest that *S. meliloti* relies on a suite of functions including peptide transporters, the bacterial envelope structures and stress response regulators to resist the aggressive assault of NCR peptides in the nodule cells.

Importance

The nitrogen fixing symbiosis of legumes with rhizobium bacteria has a predominant ecological role in the nitrogen cycle and has the potential to provide the nitrogen required for plant growth in agriculture. The host plants allow the rhizobia to colonize specific symbiotic organs, the nodules, in large numbers in order to produce sufficient reduced nitrogen for the plant needs. Some legumes, including *Medicago* spp., produce massively antimicrobial peptides to keep this large bacterial population in check. These peptides, known as NCRs, have the potential to kill the rhizobia but in nodules, they rather inhibit the division of the bacteria, which maintain a high nitrogen fixing activity. In this study, we show that the tempering of the antimicrobial activity of the NCR peptides in the *Medicago* symbiont *Sinorhizobium meliloti* is multifactorial and requires the YejABEF peptide transporter, the lipopolysaccharide outer membrane composition and the stress response regulator RpoH1.

53 **Introduction**

54 Antimicrobial peptides (AMPs) are essential mediators of innate immunity in eukaryotes. Their
55 function is to attack and kill harmful invading microbes. Animals deficient in a specific AMP or in the
56 regulation of AMP expression are more sensitive to bacterial or fungal infections, while the ectopic
57 expression of AMPs in animals and plants enhances resistance (1–3). Many organisms have also
58 recruited AMPs as essential regulators of bacteria in symbiotic associations (2). In symbiosis, hosts
59 intentionally maintain bacterial partners and the role of "symbiotic" AMPs is therefore not to
60 eradicate the symbiotic microbes but rather to police them or to optimize their metabolic integration
61 with the hosts (2, 4).

62 An extreme case of deployment of AMPs for controlling endosymbiont populations, involving
63 hundreds of peptides, is described in the rhizobium-legume symbiosis (2, 5–9). Legumes form a
64 symbiosis with phylogenetically diverse nitrogen-fixing soil bacteria, collectively called rhizobia. This
65 nutritional symbiosis provides reduced nitrogen to the plants, enabling them to grow in nitrogen-
66 poor soils. The symbiosis implies the formation of nodules, specific symbiotic organs, on the roots of
67 the plants. These nodules house the nitrogen-fixing rhizobia, which transfer their produced ammonia
68 to the plant in return for the exclusive niche in the nodules where they multiply massively from a
69 single or very few infecting bacteria to a population of millions.

70 After endocytic uptake by the symbiotic nodule cells, the multiplied bacteria reside intracellularly in
71 vesicles called symbiosomes. The nodule cells and symbiosomes establish the optimal conditions for
72 nitrogen fixation and metabolic exchange with the endosymbionts and at the same time, keep them
73 in check. The low oxygen levels prevailing in the symbiotic nodule cells transform the rhizobia into a
74 differentiated physiological state, called bacteroid, which is adapted for nitrogen fixation. Moreover,
75 in certain legume clades like the Inverted Repeat Lacking Clade (IRLC) and the Dalbergioids, the
76 physiological transition of the bacteroids is accompanied with a remarkable differentiation process
77 that is manifested in an irreversible loss of the capacity of bacteroids to divide (10, 11). These
78 terminally differentiated bacteroids have a partially permeabilized cell membrane. They are giant
79 bacterial cells. A switch in the bacterial cell cycle, from a regular succession of replication and division
80 to a series of repeated genome replications without divisions, drives this cell enlargement, resulting
81 in polyploid bacteroids.

82 The terminal differentiation is triggered by a family of Nodule-specific Cysteine-Rich peptides (NCRs),
83 produced by the symbiotic nodule cells (11–13). Over 600 *NCR* genes were identified in the *Medicago*
84 *truncatula* genome, while the NCR repertoire in other species of the IRLC and the Dalbergoids ranges
85 from a few to several hundred (11, 12, 14). The *NCR* genes in *M. truncatula* are specifically expressed
86 in the symbiotic cells (15). They are activated in waves during the differentiation of the bacteroids,
87 including sets of *NCR* genes activated at the onset and others at the intermediate or final stages of

88 the differentiation. These temporal profiles indicate that the *NCR* genes have specific functions
89 during the bacteroid formation process.
90 The NCR peptides have structural features shared with AMPs and at least some NCRs, in particular
91 the cationic ones, can kill or inhibit *in vitro* the growth of not only the rhizobium symbionts but also
92 many other bacteria and even fungi (16). Their major antibacterial activity results from their capacity
93 to disturb the integrity of the inner and outer membranes of bacteria (13, 17), although some NCRs
94 also have inhibiting activities on essential intracellular machineries (18). However, bacteroids remain
95 metabolically active for a very long time, despite the high burden of NCRs. Possibly, the environment
96 of the symbiotic nodule cells and symbiosomes contributes to tempering the antimicrobial activity of
97 the peptides. Importantly, also specific functions of the bacteria themselves are NCR-resistance
98 determinants in the bacteroids.
99 *Sinorhizobium meliloti*, the symbiont of *Medicago* plants, requires the peptide transporter BacA to
100 counter the NCR peptides inside the symbiotic nodule cells and establish a chronic infection (19). *S.*
101 *meliloti bacA* mutants are hypersensitive to the antimicrobial NCRs. They induce nodules and infect
102 plant cells seemingly normally but the mutants die rapidly after their release in the symbiotic cells.
103 This death can be avoided by blocking NCR transport to the infecting rhizobia in the *M. truncatula*
104 *dnf1* mutant (19). BacA proteins are broad-specificity peptide uptake transporters (20–22). They can
105 promote the uptake of NCR peptides, suggesting that BacA provides resistance by redirecting the
106 peptides away from the bacterial membrane, thereby limiting membrane damage. Exopolysaccharide
107 (EPS) is another known factor of *S. meliloti* that helps the endosymbionts to withstand the NCRs (14,
108 23). This negatively charged extracellular polysaccharide traps the cationic AMPs, reducing their
109 effective concentration in the membrane vicinity.
110 Bacterial resistance to AMPs is usually multifactorial (24), suggesting that besides BacA and EPS,
111 additional functions of *S. meliloti* bacteroids contribute to resisting the NCRs in the symbiotic nodule
112 cells. The literature on *S. meliloti* is rich in the description of bacterial genes that are required for
113 symbiosis. However, the reporting on these mutants often lacks precise information on their
114 bacteroid phenotype and/or on their sensitivity to NCRs. Moreover, transcriptome and Tn-seq
115 (transposon sequencing) analyses of NCR-treated cells and NCR-protein interaction studies identified
116 a whole suite of additional candidate NCR-responsive functions in *S. meliloti* (18, 25–27). Together
117 with BacA and EPS, some of these *S. meliloti* functions may contribute to alleviate the NCR stress on
118 the bacteroids. To test this hypothesis, we have selected in the present study three candidate
119 functions and analyzed the phenotype of the corresponding mutants in NCR resistance and bacteroid
120 formation.

121 **Results**

122 ***Sinorhizobium meliloti* mutants with enhanced sensitivity to NCR peptides**

123 The *S. meliloti* functions selected in this study include a broad-specificity peptide uptake transporter
124 encoded by the *yejABEF* genes (SMc02829-SMc02832), lipopolysaccharide (LPS) modifications
125 mediated by *lpsB* (SMc01219) and *lpxXL* (SMc04268) as well as *rpoH1* (SMc00646), encoding a stress
126 sigma factor. The YejABEF ABC transporter was selected on the basis of a genetic screen by Tn-seq in
127 *S. meliloti* revealing that mutants have an increased sensitivity to the peptide NCR247 (25). LPS
128 structure is one of the major determinants of AMP resistance and sensitivity in Gram-negative
129 bacteria (24, 28). The selected genes *lpsB* and *lpxXL* encode a glycosyltransferase involved in the
130 synthesis of the LPS core and a very-long-chain fatty acid acyltransferase involved in the biosynthesis
131 of lipid A, respectively. Mutants in these genes are affected in resistance to AMPs and in symbiosis
132 (29, 30). Finally, the *rpoH1* gene is a global stress response regulator in *S. meliloti* (31). This gene as
133 well as its target genes are upregulated in NCR247 treated cells (26, 27). An *rpoH1* mutant is also
134 affected in symbiosis (32). These selected genes are expressed in nodules, with peak expression in
135 different regions of the nodule where bacteria infect plant cells, undergo the differentiation process
136 or fix nitrogen (15, 33)(Fig. S1).

137 The sensitivity of mutants in these candidate genes was tested with a small panel of cationic NCR
138 peptides that were previously shown to have antimicrobial activity (14). The tested peptides, NCR169
139 (isoelectric point 8.45), NCR183 (10.10), NCR247 (10.15) and NCR280 (9.80), displayed three different
140 expression patterns in the nodule tissues (15). The *NCR280* gene is expressed in the younger nodule
141 cells, the *NCR169* gene in the older cells while *NCR183* and *NCR247* have an intermediate expression
142 pattern (Fig. S1). The selected mutants were tested along with the wild-type strain and the *bacA*
143 mutant, which was previously shown to be hypersensitive to NCRs (19). The four tested NCR peptides
144 had a strong antimicrobial activity against the wild-type strain, which displayed a survival rate
145 ranging from 8% to 0.03% depending on the tested peptide (Table S1). In agreement with previous
146 results, the *bacA* mutant was hypersensitive to the four peptides (Table S1; Fig. 1). Interestingly, the
147 newly analyzed mutants all displayed a higher sensitivity to at least one of the peptides compared to
148 the wild type (Table S1; Fig. 1). The *lpxXL* mutant was more sensitive to the four peptides, the *lpsB*,
149 *yejE* and *yejF* mutants were more sensitive to NCR183, NCR247 and NCR280. The *yejA* mutant was
150 more sensitive to NCR280 and the *rpoH1* mutant was more sensitive to NCR247. The differential
151 response towards peptide NCR247 of the *yejA* mutant on the one hand and the *yejE* and *yejF*
152 mutants on the other hand, corresponds to the previously described Tn-seq screen with this peptide
153 (25). Contrary to the other mutants, the mutants in the YejABEF transporter genes were newly
154 constructed and not characterized before. Therefore, we confirmed that the NCR247 sensitivity
155 phenotype was directly attributable to the inactivation of the transporter by complementation of the

156 *yejF* mutant phenotype with a plasmid-borne copy of the *yejABEF* genes (Table S1). Taken together,
157 our analysis indicated that each mutant displayed a specific sensitivity profile to the panel of tested
158 peptides.
159 Besides the exposure to the NCR peptides, inside the nodules bacteroids also experience additional
160 stress factors such as elevated hydrogen peroxide levels (34), an acidic pH formed in the
161 peribacteroid space (35) and a microaerobic environment (36). Almost all the mutants behaved very
162 similar to wild type during unstressed growth in culture or in response to hydrogen peroxide, acid,
163 and low oxygen stress (Fig. S2). Only the *rpoH1* mutant was much less resistant to acid and anaerobic
164 stress and had a reduced growth rate (Fig. S2). On the other hand, the mutants were more sensitive
165 than wild type to the exposure to the detergent sodium dodecyl sulfate (SDS) (Fig. S2), indicating that
166 these mutants have a reduced ability to cope with membrane permeabilizing stresses, in agreement
167 with their increased NCR sensitivity. Thus, except for the *rpoH1* mutant, which has a general defect in
168 growth and stress management, the selected mutants seem to be, among the known stress factors in
169 the nodule environment, specifically sensitive to the NCRs.
170
171 **Nodule formation by NCR-sensitive *Sinorhizobium meliloti* mutants**
172 Next, the phenotype of these mutants in symbiosis with *M. truncatula* was compared with the wild-
173 type strain and the *bacA* mutant. Measurement of the nitrogen fixation activity and macroscopic
174 inspection of the root system of plants inoculated with the wild type and the seven mutants (Fig. S3)
175 revealed that, besides the wild type, mutants in the *yejA*, *yejE*, *yejF* and *lpxXL* genes formed
176 functional nodules (Fix^+), although the *yejE*, *yejF* and *lpxXL* mutants had a reduced nitrogen-fixation
177 activity. On the other hand, the *bacA*, *lpsB* and *rpoH* mutants formed non-functional (Fix^-) and
178 abnormally looking nodules that were small and white, in agreement with previous descriptions (19,
179 29, 32).
180 The histological organization of the nodules formed by the mutants, the formation of infected
181 symbiotic cells and the viability of the bacteria they contain, were analysed using confocal
182 microscopy (Fig. 2A). The used staining procedure highlights the nodule bacteria with a green
183 fluorescence signal (SYTO™9) when their membranes are well preserved and with a red fluorescence
184 (propidium iodide) when their membranes are highly permeable. As previously reported, wild-type
185 nodules formed symbiotic cells infected with green-labelled elongated bacteroids, while the nodules
186 infected with the *bacA* mutant contained symbiotic cells carrying small undifferentiated bacteria
187 stained red (19).
188 Contrary to what we expected from the macroscopic inspection of the nodules and their ability to fix
189 nitrogen, the *yejA*, *yejE* and *yejF* mutant bacteroids were substantially altered compared to wild-type
190 bacteroids. A high proportion of them were red-stained indicating that their membranes were

191 strongly permeabilized. Nevertheless, other host cells contained bacteroids stained in green by the
192 SYTO^{TM}9 dye. LpxXL is known to be important, but not essential to *S. meliloti* during symbiosis with
193 alfalfa (*Medicago sativa*) (37). The mutant forms hypertrophied bacteroids (30). In our experiments,
194 the *lpxXL* mutant displayed elongated bacteroids but mostly permeable to propidium iodide (stained
195 in red). This observation confirmed that *S. meliloti* LpxXL is also essential for the normal bacteroid
196 differentiation process in *M. truncatula* but that it is not crucial for infection and nitrogen fixation.
197 The *rpoH1* mutant formed elongated bacteroids that nevertheless were strongly stained by
198 propidium iodide, in agreement with the Fix^{-} phenotype of the nodules and the described phenotype
199 of the mutant in alfalfa (32). Inside the small bumps elicited by the *lpsB* mutant, no cell seems to be
200 colonised by bacteria as revealed by confocal microscopy. Thus, the *S. meliloti lpsB* mutant failed to
201 colonize the host cells and was defective at a stage before plant cell infection. It was previously
202 reported that the *lpsB* mutant colonizes nodules cells in *M. sativa* suggesting a more severe defect in
203 *M. truncatula* (38, 39). Therefore, we tested the phenotype of the selected mutants also on *M. sativa*
204 (Fig. S4). The *lpsB*, *rpoH1* and the *yejA* mutants had indeed milder defects on this host while the
205 other mutants had similar phenotypes on the two hosts.
206
207 **Can the increased membrane permeability of the NCR-sensitive *Sinorhizobium meliloti* mutants be**
208 **attributed to the NCRs in nodules?**
209 The high membrane permeability of the *bacA* mutant nodule bacteria is the result of the action of
210 the NCR peptides in the nodule cells on this NCR-hypersensitive mutant (19). Possibly, the same is
211 true for the other mutants. To test this hypothesis, we made use of the *M. truncatula dnf1* mutant,
212 which is defective in a nodule-specific subunit of the signal peptidase complex (40). This mutant
213 cannot transport NCR peptides to the symbiosomes (13). As a result, the wild-type *S. meliloti* nodule
214 bacteria in this mutant are not differentiated. The *bacA* mutant, which is strongly permeabilized and
215 stained by propidium iodide in nodules of wild-type *M. truncatula* plants, is not so in the *dnf1* mutant
216 nodule cells because the bacteria are not challenged anymore with the NCRs (Fig. 2B)(19). Similarly
217 to the *bacA* mutant, the *yejA*, *yejE*, *yejF*, *lpxXL* and *rpoH1* mutants did not display membrane
218 permeability, as revealed by the absence of propidium iodide staining, in the infected nodule cells of
219 the *dnf1* mutant (Fig. 2B). This thus suggests that these mutants become membrane-permeabilized
220 by the action of the NCRs and that their symbiotic defects are at least in part due to their
221 hypersensitivity to the NCRs. The *lpsB* mutant did not form detectable nodule-like structures on the
222 *dnf1* roots. Therefore, we cannot conclude on the involvement of the NCR peptides in the symbiotic
223 phenotype of this mutant.
224
225 **Bacteroid differentiation of the NCR-sensitive *Sinorhizobium meliloti* mutants**

226 A very strong cell enlargement and an increase in the ploidy level of the bacteria characterize the
227 differentiated bacteroids in *Medicago* nodules. These parameters can be readily measured by DAPI
228 staining and flow cytometry (10). The wild-type bacteroids from *M. truncatula* nodules had a high
229 DNA content, over twenty fold higher than the DNA content in free-living *S. meliloti* (Fig. 3) and
230 increased light-scattering parameters reflecting the cell enlargement (Fig. S5). As previously
231 reported, the nodules infected by the *bacA* mutant did not contain differentiated bacteria (Fig. 3, Fig.
232 S5)(21). The bacteria in nodules induced by the *lpsB* mutant, probably located in infection threads,
233 had a profile that confirmed the complete absence of differentiated bacteria (Fig. 3, Fig. S5). Nodules
234 infected with the *rpoH1* mutant had mostly undifferentiated bacteria although a small amount of
235 fully differentiated cells was detected, as well as cells in an intermediate stage. Also the nodules of
236 the *lpxXL* mutant contained many undifferentiated bacteria as well as fully differentiated ones (Fig. 3,
237 Fig. S5). In contrast, the *yejA*, *yejE* and *yejF* mutant nodules contained large numbers of fully
238 differentiated bacteria (Fig. 3, Fig. S5).
239 It was reported previously that the *lpxXL* mutant formed nodules containing hypertrophied and
240 larger bacteria than the wild-type bacteroids (30). In our study, this difference was detectable in the
241 flow cytometry measurements showing a higher DAPI fluorescence and light scattering for the small
242 portion of differentiated bacteria in these nodules (Fig. 3, Fig. S5). Moreover, we noticed that the
243 bacteroids in the nodules infected with the *yejA*, *yejE* and *yejF* mutants displayed similar higher DNA
244 fluorescence and light scattering (Fig. 3, Fig. S5), suggesting that also these bacteroids have abnormal
245 morphologies.
246 These patterns in *M. truncatula* nodules were overall similar in *M. sativa* although the *rpoH1* mutant
247 showed a higher number of intermediate and fully differentiated bacteroids and the *yejA* mutant had
248 a profile similar to the wild type in nodules at 21 dpi while larger than normal bacteroids were only
249 detected at 32 dpi (Fig. S6). These differences corresponded well with the macroscopic and
250 microscopic differences in the nodules between the two host plants (Fig. 2, Fig. S3, Fig. S4).
251
252 **Defective bacteroid differentiation of *yejE* and *yejF* mutants**
253 To confirm the altered bacteroid morphologies of the *yej* mutants suggested by the cytometry
254 analysis, the *yejE* and *yejF* mutants were observed at high magnification by microscopy. Confocal and
255 transmission electron microscopy of *M. sativa* nodule sections showed that the nodule cells infected
256 with the *yejE* or *yejF* mutant contained a very heterogeneous population of abnormal bacteroid
257 morphs, including elongated, spherical, club-shaped or irregular blob-like cells (Fig. 4A, Fig. S7). These
258 cells contrasted strongly with the narrow, elongated wild-type bacteroids. This aberrant bacteroid
259 phenotype of the mutants was restored to a wild-type phenotype by the introduction of a plasmid-
260 borne copy of the *yejABEF* genes (Fig. S7). The difference between wild-type and mutant bacteroids

261 was also obvious by fluorescence microscopy observations of purified nodule bacteria (Fig. 4B). The
262 quantification of cell morphology parameters by image analysis with MicrobeJ of free-living bacteria
263 and the purified nodule bacteria confirmed the irregular forms of *yejE* and *yejF* bacteroids, notably
264 showing that these bacteroids are broader and more spherical than the elongated wild-type
265 bacteroids (Fig. 4C). Transmission electron microscopy further showed that the cytoplasm and inner
266 membrane of many of the *yejF* bacteroids was retracted, leaving very large intermembrane spaces,
267 which in some cases even developed into vacuoles, entirely surrounded by cytoplasm. Some cells had
268 multiple small and large vacuoles (Fig. S7A). In contrast to the bacteroids, in the cultured bacteria, no
269 differences were observed in the ultrastructure of the wild-type and *yejF* mutant bacteria (Fig. S7B).
270 The formation of strongly abnormal bacteroids of the *yej* mutants is *a priori* contradictory with the
271 nitrogen fixation activity of these nodules. Expression of the *nifH* gene is a marker for nitrogen-fixing
272 bacteroids (41). A *GFP* gene under the control of the *nifH* promoter was introduced into the wild-
273 type strain and the *bacA* (as a negative control), *yejE* and *yejF* mutants. Analysis of the GFP
274 fluorescence in nodule bacteria of *M. truncatula* (Fig. 5) and *M. sativa* (Fig. S8) by confocal
275 microscopy and flow cytometry showed that despite their aberrant morphology, the *yejE* and *yejF*
276 bacteroids are mostly functional, although some nodule cells contain highly permeable bacteroids,
277 lacking the GFP-signal suggesting that they were non-functional.
278
279 **NCR247 uptake by the YejABEF transporter**
280 In *Escherichia coli*, both YejABEF and the BacA homolog SbmA mediate the transport of microcin C
281 peptide-nucleotide antibiotics. Therefore, we tested whether the overlap in substrates of YejABEF
282 and BacA can be extended to NCR peptides, which are known substrates of BacA (20, 21). We tested
283 the impact of the mutations in the YejABEF transporter genes on NCR247 uptake and compared it
284 with a mutation in *bacA*. With a flow cytometry based assay and a fluorescent derivative of the
285 NCR247 peptide, we found that while the NCR247 uptake is completely abolished in the *bacA*
286 mutant, as expected, its uptake is also reduced but not completely abolished in the *yejE* and *yejF*
287 mutants (Fig. 6). This suggests that the YejABEF transporter contributes to NCR uptake.
288
289 **Discussion**
290 **Multiple functions of *Sinorhizobium meliloti* contribute to NCR resistance and are required for**
291 **bacteroid formation and persistence**
292 The NCR peptides are a two-edged sword. On the one hand, they maneuver the rhizobial
293 endosymbionts into a terminally differentiated state via a multitude of activities on the bacteria from
294 which the membrane permeabilization, cell cycle perturbation (polyploidization) and cell

295 enlargement are the most visible ones. On the other hand, many NCRs have antimicrobial activity,
296 notably the cationic ones, potentially killing the endosymbionts (13, 14). Therefore, rhizobia have to
297 defend themselves to be able to establish a chronic infection in the NCR-producing symbiotic cells of
298 the nodules. Previous work has identified the BacA peptide transporter and the EPS barrier in the
299 bacterial envelope as defenses of *Sinorhizobium* strains against the NCRs of their *Medicago* hosts (14,
300 19, 23).
301 Here, we defined three new functions in *S. meliloti*, the LPS, the sigma factor RpoH1, and the YejABEF
302 peptide transporter as additional determinants in bacteroids, required to cope with the NCR
303 peptides. We show that knockout mutants in the corresponding genes are more sensitive to a panel
304 of antimicrobial NCRs and that this hypersensitivity is correlated with a strongly enhanced membrane
305 permeability of the nodule bacteria and abnormalities in their morphology and ploidy levels. It is
306 striking, however, that the different mutants have markedly different bacteroid phenotypes, ranging
307 from undifferentiated to hyper-differentiated. This can be attributed to at least three factors. Each
308 mutant has a specific NCR-sensitivity profile when tested against a small panel of peptides and the
309 "NCR landscape" present in the developing symbiotic cells is continuously changing because of the
310 expression of the *NCR* genes in different waves during symbiotic cell differentiation (15). Accordingly,
311 each mutant could accumulate NCR-induced damage at a different rate and reach the breaking point
312 at different stages over the course of the bacteroid differentiation process (Fig. S1). Moreover, the
313 expression pattern of the bacterial genes in the nodule zones is different, suggesting that their
314 principal impact is realized at distinct stages of the symbiotic cell development and bacteroid
315 differentiation.
316 Blocking the targeting of the NCR peptides to the nodule bacteria by the use of the *M. truncatula*
317 *dnf1* mutant prevents the membrane permeabilization of the nodule bacteria in the mutants. This
318 observation places the symbiotic role of these bacterial genes downstream of the peptide targeting
319 to the symbiosomes (except for *lpsB*, see below) and links them, at least in part, to the NCRs. It
320 should be noted that besides the antimicrobial NCR peptides, the other stress factors present in the
321 nodule environment, such as high H_2O_2 levels, a low pH and low oxygen (34-36), are possibly also
322 reduced or absent in the *dnf1* nodules since they are non-functional (40). However, we found that,
323 except for *rpoH1*, mutants in the studied genes were not differently affected than the wild type by
324 these stresses, making it unlikely that they are the main cause of the bacteroid phenotypes in these
325 mutants.
326 The functions of *S. meliloti* described here and before probably picture only part of the full toolkit of
327 this symbiont to survive the NCR challenge. Many additional *S. meliloti* mutants are described with
328 symbiotic phenotypes that are suggestive for a similar contribution to NCR resistance. (26, 42–53). In
329 addition, other genes that could be important for symbiosis, were discovered in a Tn-seq screen with

330 the peptide NCR247 (25). This screen identified here-described functions like the BacA and YejABEF
331 transporters, the LPS and EPS biosynthesis, but also never analyzed functions. It would be of major
332 interest to explore the function of these genes in relation to the NCR response of bacteroids. Note
333 that some of these genes might have escaped identification in previous genetic screens for symbiosis
334 mutants because mutations might provoke only subtle phenotypes with a weak overall effect on
335 nitrogen fixation in standard laboratory conditions but with bacteroid alterations in morphology and
336 persistence as illustrated here with the *yejABEF* mutants.
337
338 **Response to NCR-induced stress regulated by the alternative sigma factor RpoH1**
339 Bacteria deal with different types of stress conditions by global transcriptional responses mediated
340 by alternative sigma factors. As a general classification, the RpoH sigma factors are believed to
341 control cytoplasmic stress responses, while the RpoE sigma factors are known to respond to
342 periplasmic and membrane stress (54). Given the membrane damage provoked by NCRs and the
343 general function of RpoE sigma factors in envelope stress response, including in response to AMPs
344 (55), a role of the RpoE regulators of *S. meliloti* in bacteroid differentiation and NCR response could *a*
345 *priori* have been expected. *S. meliloti* has 11 RpoE-like sigma factors. Remarkably, despite the fact
346 that some RpoEs have a considerable effect on gene transcription, all single mutants, all possible
347 double mutants and even a mutant lacking all 11 genes showed no detectable phenotypic difference
348 with wild type in symbiosis or during many tested free-living growth conditions, including growth in
349 the presence of membrane stresses (56, 57). Thus, the 11 *S. meliloti* RpoEs do not have the expected
350 role in regulating the envelope stress response.
351 This role seems to be taken up in part by RpoH in *S. meliloti*, in agreement with its role in symbiosis
352 and NCR resistance and the observation that growth of the *rpoH1* mutant is affected in the presence
353 of various membrane-disrupting agents (32). The latter suggests that RpoH in *S. meliloti* is not
354 respecting the canonical division of labor between alternative sigma factors and that its function is
355 not restricted to cytoplasmic stress, including acidic stress and anoxia or microoxia, but also
356 encompasses membrane stresses. We propose that the here uncovered role of RpoH1 in NCR
357 resistance and in bacteroid differentiation is connected to its regulation of membrane stress.
358
359 **The lipopolysaccharide barrier against NCR membrane damage**
360 In Gram-negative bacteria, including rhizobia, LPS constitutes the first point of attack of cationic
361 AMPs. In a two-stage process, AMPs make first electrostatic interactions with the negatively charged
362 LPS, allowing the AMPs to approach the membrane lipids and subsequently to insert into the lipid
363 bilayer, perforate it and translocate into the periplasm (58). The chemical composition of LPS can
364 influence the efficiency of the AMP attack and pathogens have evolved mechanisms to recognize the

365 presence of AMPs and to modify in response the composition of the LPS to lower the potency of the
366 AMP attack (59).
367 *S. meliloti lpsB* encodes a glycosyl transferase that participates in the biosynthesis of the LPS core
368 (60). The mutation of the gene affects both the core structure and O-antigen polymerization (41, 42).
369 The O-antigen is thought to be a camouflage, masking the membrane and the charges in the
370 membrane vicinity. In the *lpsB* mutant, the shorter O-antigen could be a less efficient shield against
371 the NCRs, offering to the peptides an easier access to membrane-proximal charges resulting in the
372 increased sensitivity of the *lpsB* mutant to the NCRs (this work) as well as to other AMPs (29, 39).
373 The *lpsB* mutant forms nodules on *M. sativa*, which contain infected cells and it has a phenotype that
374 is similar to the *bacA* mutant. However, the *lpsB* mutant forms uninfected nodules on *M. truncatula*
375 roots. Therefore, it was not possible to test the implication of NCRs in this symbiotic phenotype with
376 the use of the *dnf1* mutant, since the *DNF1* gene is expressed only in infected nodule cells (40). Since
377 the *NCR* genes are nearly exclusively expressed in the infected symbiotic cells (15), the blockage of
378 the mutant before the release of bacteria into nodule cells suggests that the LPS could provide
379 protection against another stressor produced very early on in the infection process in *M. truncatula*.
380 On the other hand, it was recently reported that some *NCR* genes are expressed in infected root hairs
381 or Nod factor-stimulated root epidermal cells (61, 62). Thus, it is possible that the challenge with
382 these early NCR peptides is already detrimental to the mutant, blocking any further progress in the
383 infection process.
384 LpxXL is a specific acyl transferase that introduces in the lipid A moiety of LPS the very long chain
385 fatty acid 27-OHC28:0 (37). This LpxXL-dependent acylation is expected to make the lipid A
386 hydrophobic, forming the biophysical basis for LpxXL-dependent NCR resistance. Hydrophobic lipid A
387 increases the thickness of the outer layer of the outer membrane and reduces the membrane
388 fluidity, which on its turn prevents or delays AMP insertion and membrane damage. Increasing lipid A
389 hydrophobicity by introducing additional acyl chains is a well-known mechanism used by *Salmonella*
390 to enhance its resistance against host AMPs during infection (59).
391
392 **The YejABEF peptide transporter provides resistance to membrane-damaging peptides and**
393 **sensitizes bacteria to AMPs with intracellular targets**
394 The YejABEF ABC transporter has never been analyzed before in the context of the rhizobium-legume
395 symbiosis. Furthermore, even though this transporter is highly conserved among proteobacteria, its
396 physiological role in whichever bacterium has been characterized only in a few instances. One of
397 them is the uptake of microcin C in *E. coli*. This translation-inhibiting peptide-nucleotide of bacterial
398 origin has no action on the bacterial membrane but has an intracellular target, the Asp aminoacyl-
399 tRNA synthase (63). A mutant in the YejABEF transporter cannot uptake microcin C and is resistant to

400 it (64, 65). Conversely, the *Salmonella* and *Brucella yejABEF* mutants are more sensitive to peptides
401 with membrane-damaging activity such as defensins, polymyxin B, protamine and melittin.
402 Consequently, these mutants have reduced pathogenicity because their capacity to survive in
403 macrophage cell lines or in mice is diminished (66, 67). Thus, the increased sensitivity of the *yejA*,
404 *yejE* and *yejF* mutants of *S. meliloti* towards NCRs is consistent with these previous findings.
405 The characteristics of the YejABEF peptide transporter towards membrane-damaging peptides versus
406 peptides with intracellular action are intriguingly parallel to the features of the BacA peptide
407 transporter (SbmA in *E. coli* and *Salmonella*). These latter transporters are required for the import of
408 diverse peptides with intracellular targets (microcins B17 and J25, Bac7, Bac5 and bleomycin) and
409 mutants are therefore resistant to them while the same mutants are hypersensitive to membrane-
410 active peptides (defensins, NCRs) (19, 68, 69, 70, 71). Moreover, the range of peptides that can be
411 imported overlap between these two transporters. Both, YejABEF and SbmA can uptake microcin C
412 derivatives (64). Furthermore, we show that both BacA and YejABEF contribute to NCR247 uptake.
413 Intriguingly, our genetic analysis suggests that both transporters cooperate to import this peptide,
414 since inactivation of one or the other abolishes or strongly reduces uptake. How these two
415 transporters can physically interact and cooperate is an issue of interest for future research.
416 Nevertheless, BacA can function (partially) in the absence of YejABEF while the inverse is not the
417 case. This could be the basis for the markedly different symbiotic phenotype of the *bacA* and *yej*
418 mutants. While the *bacA* mutation is detrimental from the earliest contact with NCRs and bacteria
419 die as soon as they are released from infection threads in the symbiotic cells, the *yej* mutants cope
420 with the NCR peptides much longer and show abnormalities only at the end of the bacteroid
421 differentiation process and symbiont lifespan. The *yejA* gene encodes the periplasmic binding protein
422 of the transporter. The *yejA* mutant had a different NCR sensitivity profile than the *yejE* and *yejF*
423 mutant and this was correlated with a different symbiotic phenotype in the *M. sativa* host. This
424 suggest that YejA contributes to the interaction with only a subset of the NCR peptides.
425 How do the YejABEF and BacA transporters contribute to resistance to NCRs and other membrane-
426 damaging peptides? The most straightforward model that has been proposed before for BacA (19–
427 21) as well as for the unrelated SapABCDF peptide uptake transporter (72), is the reduction of the
428 AMP concentration in the vicinity of the inner membrane below a critical threshold. Alternatively, the
429 presence or activity of the transporters might indirectly affect the bacterial envelope structure,
430 rendering it more robust against AMPs. The higher sensitivity of the *yej* mutants towards SDS is in
431 agreement with this possibility. Similarly, membrane alterations were reported in the *bacA* mutant of
432 *S. meliloti* (73).
433
434 **Conclusions**

435 The multifaceted NCR resistance required for symbiosis and chronic infection of the nodule cells
436 mirrors the multitude of AMP resistance mechanisms in animal pathogens, which collectively
437 contribute to the pathogenicity of these bacteria (2, 3, 74). However, one dimension of this strategy
438 in pathogens is not known in *S. meliloti* and consists of the direct recognition of host AMPs by
439 receptors triggering an adaptive response. Probably the best-studied AMP receptor is the two-
440 component regulator PhoPQ in *Salmonella*, which adjusts the LPS composition in response to the
441 presence of host peptides (59). Perhaps the *S. meliloti* ExoS-ChvI or FeuP-FeuQ two-component
442 regulators, which are upregulated by NCR treatment and essential for symbiosis (26, 42, 43), form
443 such a regulatory module, recognizing NCRs and controlling an appropriate response in the symbiotic
444 nodule cells. In this respect, it is of interest to note that the rhizobial LPS structure changes strongly
445 in bacteroids of NCR-producing nodules (75, 76).
446 As shown here, rhizobia have to defend themselves to be able to establish a chronic infection in the
447 NCR-producing symbiotic cells of the nodules. On the other hand, the profile of NCR peptides
448 produced in the nodule cells is also determinant for the outcome of the symbiosis and some *M.*
449 *truncatula* mutants in individual *NCR* genes or *M. truncatula* accessions, expressing specific *NCR*
450 alleles, display incompatibility with *S. meliloti* strains (77–80). Thus, a fine balance must be
451 established in the symbiotic nodule cells between the NCR landscapes and matching multifactorial
452 bacterial countermeasures. Perturbations in the host or in the endosymbiont, as the ones described
453 here, affecting this equilibrium lead to a breakdown of the symbiosis.
454
455 **Materials and Methods**
456 **Bacterial strains, plant growth and nodulation assays and analysis**
457 The procedures for the growth of the *S. meliloti* Sm1021 strain and its derivatives, plant culture of
458 the *M. sativa* cultivar Gabès, the *M. truncatula* accession Jemalong A17, and the A17 *dnf1* mutant,
459 nodulation assays, acetylene reduction assays, bacteroid isolation, flow cytometry measurements
460 and confocal microscopy were performed as described before (81). Bacterial mutants in *rpoH1*, *yejA*,
461 *yejE* and *yejF* were obtained by plasmid insertion and gene deletion (Table S2) as described before
462 (82). A fragment containing the *yejABEF* genes was PCR-amplified from *S. meliloti* Sm1021 genomic
463 DNA using primers yejA_NdeI_F and yejF_XbaI_R (Table S2) and cloned between the NdeI and XbaI
464 restriction sites of the pSRK(Gm) vector (83). The construct was confirmed by restriction analysis and
465 sequencing. The plasmid as well as the empty pSRK(Gm) vector were conjugated to wild type
466 Sm1021 as well as the *yejA*, *yejE*, and *yejF* mutants bi tri-parental mating (82).
467 Quantitative analysis of the shape of free-living bacteria and bacteroids was performed with the
468 MicrobeJ plugin of ImageJ (84). Bacteroid extracts and exponential phase cultures were stained with
469 2.5 nM SYTO™9 for 10 minutes at 37°C and mounted between slide and coverslip. Bacteria imaging

470 was performed on a SP8 laser scanning confocal microscope (Leica microsystems) equipped with
471 hybrid detectors and a 63x oil immersion objective (Plan Apo, NA: 1.4, Leica). For each condition,
472 multiple z-stacks (2.7 µm width, 0.7 µm step) were automatically acquired (excitation: 488 nm;
473 collection of fluorescence: 520-580 nm). Stacks were transformed as maximum intensity projections
474 using ImageJ software (85). Bacteria in the image stacks were automatically detected with MicrobeJ
475 using an intensity based threshold method with a combination of morphological filters. To ensure
476 high data quality every image was manually checked to remove false positive objects (mainly plant
477 residues). Morphological parameters were directly extracted from MicrobeJ and figures were created
478 with Excel or ggplot2 in R.
479
480 ***In vitro* sensitivity and peptide uptake assays**
481 NCR sensitivity assays were carried out essentially as described (20). Triplicate measurements were
482 performed in at least two independent experiments per treatment. Nonparametric Kruskal-Wallis
483 and post-hoc Dunn tests were performed to assess significance of differences between the sensitivity
484 of the wild type and the mutant strains. To measure the resistance of strains to sodium dodecyl
485 sulfate (SDS), H_2O_2 and HCl stress, overnight cultures of the wild type and mutants were diluted to
486 OD_{600}=0.2. A total of 100 µL of these suspensions was added to 3 ml soft agar (0.7% agar) and poured
487 onto standard 1.5% agar plates. After solidification of the soft agar, filter paper disks (5 mm
488 diameter) were placed on the center of the plate, and 5 µL of 10% (w/v) SDS, 2 M HCl or 1% H_2O_2 was
489 added to the disks. Plates were incubated at 28°C for 3 days, and the diameter of the clearing zone
490 was measured. For microaerobic and anaerobic treatments, cultures of the wild type and mutants
491 were diluted to OD_{600}=0.1 and 5-fold dilution series were prepared of each. The dilution series were
492 subsequently spotted (5 µL per spot) on agar plates. One series of plates was grown in standard
493 aerobic conditions. A second series of plates was placed in a 2.5 L airtight jar containing an
494 AnaeroPack-MicroAero (Mitsubishi Gas Chemical) bag for microaerobic growth (6-12% O_2 according
495 to the product specifications). The third series of plates was placed in a 2,5 L jar containing an
496 AnaeroGen 2,5L (Thermo Scientific) bag for anaerobic growth (<0,1% O_2 according to the product
497 specifications). All plates were grown at 28°C and after 3 days, the plates were removed from the jars
498 for the microaerobic and anaerobic conditions. After 3 days, colonies were sufficiently grown in the
499 aerobic condition for counting. Growth was observed in the microaerobic condition but less strong
500 than in the aerobic condition and these plates were further incubated for 1 day before colony
501 counting. No growth was observed after 3 days in the anaerobic condition and plates were incubated
502 for 4 days in aerobic condition before colony counting. Colony counting was done using a binocular.
503 Quadruplate measurements and two independent experiments per treatment were performed.
504 Nonparametric Kruskal-Wallis and post-hoc Dunn tests were performed to assess significance of

differences in all the assays. For growth curves, precultures were diluted to OD_{600}=0.04 in YEB medium (81). Cultures were dispatched in microtiter plates with 200 µL of culture per well. The plates were incubated in a SPECTROstar Nano (BMG Labtech) plate reader during 100 h, at 28°C, 100 rpm shaking and OD_{600} measurements every 30 min. Doubling times were calculated from the obtained growth curves (n=10) and nonparametric Kruskal-Wallis and post-hoc Dunn tests were performed to assess significance of differences between growth rates. Peptide uptake assays were performed as described in quadruplicate (20, 86).

TEM

Bacterial suspensions at OD_{600}=6 or 21 days old nodule samples were incubated in fixative (3% glutaraldehyde, 1% paraformaldehyde in 0.1 M cacodylate, pH 6.8) for one to three hours, and washed with 0.1 M cacodylate buffer, pH 6.8. Samples were then incubated one hour in 1% osmium tetroxide, 1.5% potassium ferrocyanide in water. After washing, bacterial suspensions were pelleted in 2% low melting point agarose to facilitate their manipulation. Samples were dehydrated by incubation in increasing concentrations of ethanol (nodule samples for a total of 4 hours in 10-20-30-50-70-90-100%-absolute ethanol-propylene oxide; bacterial pellets for a total of 2 hours in 10-30-50-70-90-100%-absolute ethanol), followed by infiltration with epoxy resin (low viscosity Premix Kit medium, Agar) (for nodule samples, 3 days of infiltration; for bacterial pellets, 24h of infiltration) and polymerization for 24h at 60°C. Ultrathin sections (80-70 nm) were obtained with an ultramicrotome EM UC6 (Leica Microsystems) and collected on formvar carbon-coated copper grids (Agar). Sections were stained with 2% uranyl acetate (Merck) and lead citrate (Agar) before observation with a JEOL JEM-1400 transmission electron microscope operating at 120kV. Images were acquired using a postcolumn high-resolution (11 megapixels) high-speed camera (SC1000 Orius; Gatan) and processed with Digital Micrograph (Gatan).

Acknowledgements

We are grateful to Corinne Foucault for assistance with plant experiments and Cynthia Dupas for help with the TEM experiments. QN and SD were supported by PhD fellowships from the Paris-Saclay University and QB and NB by Post-doc grants from the Agence Nationale de la Recherche. The present work has benefited from Imagerie-Gif core facility supported by the Agence Nationale de la Recherche (ANR-11-EQPX-0029/Morphoscope, ANR-10-INBS-04/FranceBioImaging; ANR-11-IDEX-0003-02/Saclay Plant Sciences). The EK laboratory is supported by the NKFIH Frontline Research project KKP129924 and a Balzan research grant. The work in the PM laboratory was supported by the LabEx Saclay Plant Sciences-SPS and grants ANR-17-CE20-0011 and ANR-16-CE20-0013 from the Agence Nationale de la Recherche.

540

541 **Author contributions**

542 QN, QB and NB have initiated jointly this work. QN, QB, NB, SD, DT, ML, EB and TT constructed strains
543 and performed nodulation assays. QN, QB, SD, RLB, CB and TT performed microscopy and flow
544 cytometry. QB, SJ, AK and EK performed the *in vitro* experiments and provided reagents. QN, QB, NB,
545 EB, TT, BA and PM conceived the study and analyzed the data. PM wrote the manuscript with input
546 from all authors.

547 **References**

548 1. Hanson MA, Lemaitre B. 2020. New insights on *Drosophila* antimicrobial peptide function in host
549 defense and beyond. Curr Opin Immunol 62:22–30.
550 2. Mergaert P. 2018. Role of antimicrobial peptides in controlling symbiotic bacterial populations.
551 Nat Prod Rep 35:336–356.
552 3. Maróti G, Kereszt A, Kondorosi E, Mergaert P. 2011. Natural roles of antimicrobial peptides in
553 microbes, plants and animals. Res Microbiol 162:363–374.
554 4. Mergaert P, Kikuchi Y, Shigenobu S, Nowack ECM. 2017. Metabolic integration of bacterial
555 endosymbionts through antimicrobial peptides. Trends Microbiol 25:703–712.
556 5. Kondorosi E, Mergaert P, Kereszt A. 2013. A paradigm for endosymbiotic life: cell differentiation
557 of *Rhizobium* bacteria provoked by host plant factors. Annu Rev Microbiol 67:611–628.
558 6. Alunni B, Gourion B. 2016. Terminal bacteroid differentiation in the legume-rhizobium symbiosis:
559 nodule-specific cysteine-rich peptides and beyond. New Phytol 211:411–417.
560 7. Pan H, Wang D. 2017. Nodule cysteine-rich peptides maintain a working balance during nitrogen-
561 fixing symbiosis. Nat Plants 3:17048.
562 8. Stonoha-Arther C, Wang D. 2018. Tough love: accommodating intracellular bacteria through
563 directed secretion of antimicrobial peptides during the nitrogen-fixing symbiosis. Curr Opin Plant
564 Biol 44:155–163.
565 9. Roy P, Achom M, Wilkinson H, Lagunas B, Gifford ML. 2020. Symbiotic outcome modified by the
566 diversification from 7 to over 700 nodule-specific cysteine-rich peptides. Genes 11:348.
567 10. Mergaert P, Uchiumi T, Alunni B, Evanno G, Cheron A, Catrice O, Mausset A-E, Barloy-Hubler F,
568 Galibert F, Kondorosi A, Kondorosi E. 2006. Eukaryotic control on bacterial cell cycle and
569 differentiation in the *Rhizobium*-legume symbiosis. Proc Natl Acad Sci USA 103:5230–5235.
570 11. Czernic P, Gully D, Cartieaux F, Moulin L, Guefrachi I, Patrel D, Pierre O, Fardoux J, Chaintreuil C,
571 Nguyen P, Gressent F, Da Silva C, Poulain J, Wincker P, Rofidal V, Hem S, Barrière Q, Arrighi J-F,
572 Mergaert P, Giraud E. 2015. Convergent evolution of endosymbiont differentiation in Dalbergioid
573 and Inverted Repeat-Lacking Clade legumes mediated by nodule-specific cysteine-rich peptides.
574 Plant Physiol 169:1254–1265.
575 12. Mergaert P, Nikovics K, Kelemen Z, Maunoury N, Vaubert D, Kondorosi A, Kondorosi E. 2003. A
576 novel family in *Medicago truncatula* consisting of more than 300 nodule-specific genes coding
577 for small, secreted polypeptides with conserved cysteine motifs. Plant Physiol 132:161–173.
578 13. Van de Velde W, Zehirov G, Szatmari A, Debreczeny M, Ishihara H, Kevei Z, Farkas A, Mikulass K,
579 Nagy A, Tiricz H, Satiat-Jeunemaître B, Alunni B, Bourge M, Kucho K, Abe M, Kereszt A, Maroti G,
580 Uchiumi T, Kondorosi E, Mergaert P. 2010. Plant peptides govern terminal differentiation of
581 bacteria in symbiosis. Science 327:1122–1126.

582 14. Montiel J, Downie JA, Farkas A, Bihari P, Herczeg R, Bálint B, Mergaert P, Kereszt A, Kondorosi É.
583 2017. Morphotype of bacteroids in different legumes correlates with the number and type of
584 symbiotic NCR peptides. Proc Natl Acad Sci USA 114:5041–5046.
585 15. Guefrachi I, Nagymihaly M, Pislariu CI, Van de Velde W, Ratet P, Mars M, Udvardi MK, Kondorosi
586 E, Mergaert P, Alunni B. 2014. Extreme specificity of *NCR* gene expression in *Medicago*
587 *truncatula*. BMC Genom 15:712.
588 16. Lima RM, Kylarová S, Mergaert P, Kondorosi É. 2020. Unexplored arsenals of legume peptides
589 with potential for their applications in medicine and agriculture. Front Microbiol 11:1307.
590 17. Mikuláss KR, Nagy K, Bogos B, Szegletes Z, Kovács E, Farkas A, Váró G, Kondorosi É, Kereszt A.
591 2016. Antimicrobial nodule-specific cysteine-rich peptides disturb the integrity of bacterial outer
592 and inner membranes and cause loss of membrane potential. Ann Clin Microbiol Antimicrob
593 15:43.
594 18. Farkas A, Maróti G, Durgő H, Györgypál Z, Lima RM, Medzihradszky KF, Kereszt A, Mergaert P,
595 Kondorosi É. 2014. *Medicago truncatula* symbiotic peptide NCR247 contributes to bacteroid
596 differentiation through multiple mechanisms. Proc Natl Acad Sci USA 111:5183–5188.
597 19. Haag AF, Baloban M, Sani M, Kerscher B, Pierre O, Farkas A, Longhi R, Boncompagni E, Hérouart
598 D, Dall'angelo S, Kondorosi E, Zanda M, Mergaert P, Ferguson GP. 2011. Protection of
599 *Sinorhizobium* against host cysteine-rich antimicrobial peptides is critical for symbiosis. PLoS Biol
600 9:e1001169.
601 20. Barrière Q, Guefrachi I, Gully D, Lamouche F, Pierre O, Fardoux J, Chaintreuil C, Alunni B,
602 Timchenko T, Giraud E, Mergaert P. 2017. Integrated roles of BclA and DD-carboxypeptidase 1 in
603 Bradyrhizobium differentiation within NCR-producing and NCR-lacking root nodules. Sci Rep
604 7:9063.
605 21. Guefrachi I, Pierre O, Timchenko T, Alunni B, Barrière Q, Czernic P, Villaécija-Aguilar J-A, Verly C,
606 Bourge M, Fardoux J, Mars M, Kondorosi E, Giraud E, Mergaert P. 2015. *Bradyrhizobium* BclA is a
607 peptide transporter required for bacterial differentiation in symbiosis with *Aeschynomene*
608 legumes. Mol Plant-Microbe Interact 28:1155–1166.
609 22. Rempel S, Gati C, Nijland M, Thangaratnarajah C, Karyolaimos A, de Gier JW, Guskov A, Slotboom
610 DJ. 2020. A mycobacterial ABC transporter mediates the uptake of hydrophilic compounds.
611 Nature 580:409–412.
612 23. Arnold MFF, Penterman J, Shabab M, Chen EJ, Walker GC. 2018. Important late-stage symbiotic
613 role of the *Sinorhizobium meliloti* exopolysaccharide succinoglycan. J Bacteriol 200:e00665-17.
614 24. Cole JN, Nizet V. 2016. Bacterial evasion of host antimicrobial peptide defenses. Microbiol
615 Spectrum 4:VMBF-0006-2015.

616 25. Arnold MFF, Shabab M, Penterman J, Boehme KL, Griffitts JS, Walker GC. 2017. Genome-wide
617 sensitivity analysis of the microsymbiont *Sinorhizobium meliloti* to symbiotically important,
618 defensin-like host peptides. mBio 8:e01060-17.
619 26. Penterman J, Abo RP, De Nisco NJ, Arnold MFF, Longhi R, Zanda M, Walker GC. 2014. Host plant
620 peptides elicit a transcriptional response to control the *Sinorhizobium meliloti* cell cycle during
621 symbiosis. Proc Natl Acad Sci USA 111:3561–3566.
622 27. Tiricz H, Szucs A, Farkas A, Pap B, Lima RM, Maróti G, Kondorosi É, Kereszt A. 2013. Antimicrobial
623 nodule-specific cysteine-rich peptides induce membrane depolarization-associated changes in
624 the transcriptome of *Sinorhizobium meliloti*. Appl Environ Microbiol 79:6737–6746.
625 28. Simpson BW, Trent MS. 2019. Pushing the envelope: LPS modifications and their consequences.
626 Nat Rev Microbiol 17:403–416.
627 29. Campbell GRO, Sharypova LA, Scheidle H, Jones KM, Niehaus K, Becker A, Walker GC. 2003.
628 Striking complexity of lipopolysaccharide defects in a collection of *Sinorhizobium meliloti*
629 mutants. J Bacteriol 185:3853–3862.
630 30. Haag AF, Wehmeier S, Beck S, Marlow VL, Fletcher V, James EK, Ferguson GP. 2009. The
631 *Sinorhizobium meliloti* LpxXL and AcpXL proteins play important roles in bacteroid development
632 within alfalfa. J Bacteriol 191:4681–4686.
633 31. Barnett MJ, Bittner AN, Toman CJ, Oke V, Long SR. 2012. Dual RpoH sigma factors and
634 transcriptional plasticity in a symbiotic bacterium. J Bacteriol 194:4983–4994.
635 32. Mitsui H, Sato T, Sato Y, Ito N, Minamisawa K. 2004. *Sinorhizobium meliloti* RpoH1 is required for
636 effective nitrogen-fixing symbiosis with alfalfa. Mol Genet Genom 271:416–425.
637 33. Roux B, Rodde N, Jardinaud M-F, Timmers T, Sauviac L, Cottret L, Carrère S, Sallet E, Courcelle E,
638 Moreau S, Debellé F, Capela D, de Carvalho-Niebel F, Gouzy J, Bruand C, Gamas P. 2014. An
639 integrated analysis of plant and bacterial gene expression in symbiotic root nodules using laser-
640 capture microdissection coupled to RNA sequencing. Plant J 77:817–837.
641 34. Santos R, Hérouart D, Sigaud S, Touati D, Puppo A. 2001. Oxidative burst in alfalfa-*Sinorhizobium*
642 *meliloti* symbiotic interaction. Mol Plant-Microbe Interact 14:86–89.
643 35. Pierre O, Engler G, Hopkins J, Brau F, Boncompagni E, Hérouart D. 2013. Peribacteroid space
644 acidification: a marker of mature bacteroid functioning in *Medicago truncatula* nodules. Plant
645 Cell Environ 36:2059-2070.
646 36. Soupène E, Foussard M, Boistard P, Truchet G, Batut J. 1995. Oxygen as a key developmental
647 regulator of *Rhizobium meliloti* N_2-fixation gene expression within the alfalfa root nodule. Proc
648 Natl Acad Sci USA 92:3759–3763.
649 37. Ferguson GP, Datta A, Carlson RW, Walker GC. 2005. Importance of unusually modified lipid A in
650 *Sinorhizobium* stress resistance and legume symbiosis. Mol Microbiol 56:68–80.

651 38. Niehaus K, Lagares A, Pühler A. 1998. A *Sinorhizobium meliloti* lipopolysaccharide mutant
652 induces effective nodules on the host plant *Medicago sativa* (alfalfa) but fails to establish a
653 symbiosis with *Medicago truncatula*. Mol Plant-Microbe Interact 11:906–914.
654 39. Campbell GRO, Reuhs BL, Walker GC. 2002. Chronic intracellular infection of alfalfa nodules by
655 *Sinorhizobium meliloti* requires correct lipopolysaccharide core. Proc Natl Acad Sci USA 99:3938–
656 3943.
657 40. Wang D, Griffitts J, Starker C, Fedorova E, Limpens E, Ivanov S, Bisseling T, Long S. 2010. A
658 nodule-specific protein secretory pathway required for nitrogen-fixing symbiosis. Science
659 327:1126–1129.
660 41. Mendoza-Suárez MA, Geddes BA, Sánchez-Cañizares C, Ramírez-González RH, Kirchhelle C, Jorrin
661 B, Poole PS. 2020. Optimizing *Rhizobium*-legume symbioses by simultaneous measurement of
662 rhizobial competitiveness and N_2 fixation in nodules. Proc Natl Acad Sci USA 117:9822–9831.
663 42. Bélanger L, Dimmick KA, Fleming JS, Charles TC. 2009. Null mutations in *Sinorhizobium meliloti*
664 *exoS* and *chvI* demonstrate the importance of this two-component regulatory system for
665 symbiosis. Mol Microbiol 74:1223–1237.
666 43. Griffitts JS, Carlyon RE, Erickson JH, Moulton JL, Barnett MJ, Toman CJ, Long SR. 2008. A
667 *Sinorhizobium meliloti* osmosensory two-component system required for cyclic glucan export
668 and symbiosis. Mol Microbiol 69:479–490.
669 44. Santos R, Hérouart D, Puppo A, Touati D. 2000. Critical protective role of bacterial superoxide
670 dismutase in rhizobium-legume symbiosis. Mol Microbiol 38:750–759.
671 45. Jamet A, Sigaud S, Van de Sype G, Puppo A, Hérouart D. 2003. Expression of the bacterial
672 catalase genes during *Sinorhizobium meliloti-Medicago sativa* symbiosis and their crucial role
673 during the infection process. Mol Plant-Microbe Interact 16:217–225.
674 46. Castro-Sowinski S, Matan O, Bonafede P, Okon Y. 2007. A thioredoxin of *Sinorhizobium meliloti*
675 CE52G is required for melanin production and symbiotic nitrogen fixation. Mol Plant-Microbe
676 Interact 20:986–993.
677 47. Benyamina SM, Baldacci-Cresp F, Couturier J, Chibani K, Hopkins J, Bekki A, de Lajudie P, Rouhier
678 N, Jacquot J-P, Alloing G, Puppo A, Frendo P. 2013. Two Sinorhizobium meliloti glutaredoxins
679 regulate iron metabolism and symbiotic bacteroid differentiation. Environ Microbiol 15:795–810.
680 48. Tang G, Li N, Liu Y, Yu L, Yan J, Luo L. 2018. *Sinorhizobium meliloti* glutathione reductase is
681 required for both redox homeostasis and symbiosis. Appl Environ Microbiol 84:e01937-17.
682 49. Yang L, El Msehli S, Benyamina S, Lambert A, Hopkins J, Cazareth J, Pierre O, Hérouart D, Achi-
683 Smiti S, Boncompagni E, Frendo P. 2020. Glutathione deficiency in *Sinorhizobium meliloti* does
684 not impair bacteroid differentiation but induces early senescence in the interaction with
685 *Medicago truncatula*. Front Plant Sci 11:137.

686 50. Tang G, Xing S, Wang S, Yu L, Li X, Staehelin C, Yang M, Luo L. 2017. Regulation of cysteine
687 residues in LsrB proteins from *Sinorhizobium meliloti* under free-living and symbiotic oxidative
688 stress. Environ Microbiol 19:5130–5145.
689 51. Bittner AN, Foltz A, Oke V. 2007. Only one of five *groEL* genes is required for viability and
690 successful symbiosis in *Sinorhizobium meliloti*. J Bacteriol 189:1884–1889.
691 52. Ogden AJ, McAleer JM, Kahn ML. 2019. Characterization of the *Sinorhizobium meliloti* HslUV and
692 ClpXP protease systems in free-living and symbiotic states. J Bacteriol 201:e00498-18.
693 53. Cosme AM, Becker A, Santos MR, Sharypova LA, Santos PM, Moreira LM. 2008. The outer
694 membrane protein TolC from *Sinorhizobium meliloti* affects protein secretion, polysaccharide
695 biosynthesis, antimicrobial resistance, and symbiosis. Mol Plant-Microbe Interact 21:947–957.
696 54. Gruber TM, Gross CA. 2003. Multiple sigma subunits and the partitioning of bacterial
697 transcription space. Annu Rev Microbiol 57:441–466.
698 55. Guest RL, Raivio TL. 2016. Role of the gram-negative envelope stress response in the presence of
699 antimicrobial agents. Trends Microbiol 24:377–390.
700 56. Sauviac L, Philippe H, Phok K, Bruand C. 2007. An extracytoplasmic function sigma factor acts as a
701 general stress response regulator in *Sinorhizobium meliloti*. J Bacteriol 189:4204–4216.
702 57. Lang C, Barnett MJ, Fisher RF, Smith LS, Diodati ME, Long SR. 2018. Most S*inorhizobium meliloti*
703 extracytoplasmic function sigma factors control accessory functions. mSphere 3:e00454-18.
704 58. Zasloff M. 2002. Antimicrobial peptides of multicellular organisms. Nature 415:389–395.
705 59. Dalebroux ZD, Miller SI. 2014. *Salmonellae* PhoPQ regulation of the outer membrane to resist
706 innate immunity. Curr Opin Microbiol 17:106–113.
707 60. Lagares A, Hozbor DF, Niehaus K, Otero AJ, Lorenzen J, Arnold W, Pühler A. 2001. Genetic
708 characterization of a Sinorhizobium meliloti chromosomal region in lipopolysaccharide
709 biosynthesis. J Bacteriol 183:1248–1258.
710 61. Jardinaud M-F, Boivin S, Rodde N, Catrice O, Kisiala A, Lepage A, Moreau S, Roux B, Cottret L,
711 Sallet E, Brault M, Emery RJN, Gouzy J, Frugier F, Gamas P. 2016. A laser dissection-RNAseq
712 analysis highlights the activation of cytokinin pathways by Nod factors in the *Medicago*
713 *truncatula* root epidermis. Plant Physiol 171:2256–2276.
714 62. Liu C-W, Breakspear A, Guan D, Cerri MR, Jackson K, Jiang S, Robson F, Radhakrishnan GV, Roy S,
715 Bone C, Stacey N, Rogers C, Trick M, Niebel A, Oldroyd GED, de Carvalho-Niebel F, Murray JD.
716 2019. NIN Acts as a network hub controlling a growth module required for rhizobial infection.
717 Plant Physiol 179:1704–1722.
718 63. Travin DY, Severinov K, Dubiley S. 2021. Natural Trojan horse inhibitors of aminoacyl-tRNA
719 sythetases. RSC Chem Biol. doi: 10.1039/D0CB00208A.

720 64. Bantysh O, Serebryakova M, Zukher I, Kulikovsky A, Tsibulskaya D, Dubiley S, Severinov K. 2015.
721 Enzymatic synthesis and functional characterization of bioactive Microcin C-like compounds with
722 altered peptide sequence and length. J Bacteriol 197:3133–3141.
723 65. Novikova M, Metlitskaya A, Datsenko K, Kazakov T, Kazakov A, Wanner B, Severinov K. 2007. The
724 *Escherichia coli* Yej transporter is required for the uptake of translation inhibitor microcin C. J
725 Bacteriol 189:8361–8365.
726 66. Eswarappa SM, Panguluri KK, Hensel M, Chakravortty D. 2008. The yejABEF operon of Salmonella
727 confers resistance to antimicrobial peptides and contributes to its virulence. Microbiology
728 154:666–678.
729 67. Wang Z, Bie P, Cheng J, Lu L, Cui B, Wu Q. 2016. The ABC transporter YejABEF is required for
730 resistance to antimicrobial peptides and the virulence of *Brucella melitensis*. Sci Rep 6:31876.
731 68. Salomón RA, Farías RN. 1995. The peptide antibiotic microcin 25 is imported through the TonB
732 pathway and the SbmA protein. J Bacteriol 177:3323–3325.
733 69 Laviña M, Pugsley AP, Moreno F. 1986. Identification, mapping, cloning and characterization of a
734 gene (sbmA) required for microcin B17 action on *Escherichia coli* K12. J Gen Microbiol 132:1685–
735 1693.
736 70. Wehmeier S, Arnold MFF, Marlow VL, Aouida M, Myka KK, Fletcher V, Benincasa M, Scocchi M,
737 Ramotar D, Ferguson GP. 2010. Internalization of a thiazole-modified peptide in *Sinorhizobium*
738 *meliloti* occurs by BacA-dependent and -independent mechanisms. Microbiology 156:2702–
739 2713.
740 71. Arnold MFF, Haag AF, Capewell S, Boshoff HI, James EK, McDonald R, Mair I, Mitchell AM,
741 Kerscher B, Mitchell TJ, Mergaert P, Barry CE, Scocchi M, Zanda M, Campopiano DJ, Ferguson GP.
742 2013. Partial complementation of *Sinorhizobium meliloti bacA* mutant phenotypes by the
743 *Mycobacterium tuberculosis* BacA protein. J Bacteriol 195:389–398.
744 72. Parra-Lopez C, Baer MT, Groisman EA. 1993. Molecular genetic analysis of a locus required for
745 resistance to antimicrobial peptides in *Salmonella typhimurium*. EMBO J 12:4053–4062.
746 73. Ferguson GP, Roop RM, Walker GC. 2002. Deficiency of a *Sinorhizobium meliloti* BacA mutant in
747 alfalfa symbiosis correlates with alteration of the cell envelope. J Bacteriol 184:5625–5632.
748 74. Bauer ME, Shafer WM. 2015. On the *in vivo* significance of bacterial resistance to antimicrobial
749 peptides. Biochim Biophys Acta 1848:3101–3111.
750 75. Kannenberg EL, Carlson RW. 2001. Lipid A and O-chain modifications cause *Rhizobium*
751 lipopolysaccharides to become hydrophobic during bacteroid development. Mol Microbiol
752 39:379–391.
753 76. Crespo-Rivas JC, Guefrachi I, Mok KC, Villaécija-Aguilar JA, Acosta-Jurado S, Pierre O, Ruiz-Sainz
754 JE, Taga ME, Mergaert P, Vinardell JM. 2016. *Sinorhizobium fredii* HH103 bacteroids are not

755 terminally differentiated and show altered O-antigen in nodules of the Inverted Repeat-Lacking
756 Clade legume *Glycyrrhiza uralensis*. Environ Microbiol 18:2392–2404.
757 77. Kim M, Chen Y, Xi J, Waters C, Chen R, Wang D. 2015. An antimicrobial peptide essential for
758 bacterial survival in the nitrogen-fixing symbiosis. Proc Natl Acad Sci USA 112:15238–15243.
759 78. Horváth B, Domonkos Á, Kereszt A, Szűcs A, Ábrahám E, Ayaydin F, Bóka K, Chen Y, Chen R,
760 Murray JD, Udvardi MK, Kondorosi É, Kaló P. 2015. Loss of the nodule-specific cysteine rich
761 peptide, NCR169, abolishes symbiotic nitrogen fixation in the *Medicago truncatula dnf7* mutant.
762 Proc Natl Acad Sci USA 112:15232–15237.
763 79. Wang Q, Yang S, Liu J, Terecskei K, Ábrahám E, Gombár A, Domonkos Á, Szűcs A, Körmöczi P,
764 Wang T, Fodor L, Mao L, Fei Z, Kondorosi É, Kaló P, Kereszt A, Zhu H. 2017. Host-secreted
765 antimicrobial peptide enforces symbiotic selectivity in *Medicago truncatula*. Proc Natl Acad Sci
766 USA 114:6854–6859.
767 80. Yang S, Wang Q, Fedorova E, Liu J, Qin Q, Zheng Q, Price PA, Pan H, Wang D, Griffitts JS, Bisseling
768 T, Zhu H. 2017. Microsymbiont discrimination mediated by a host-secreted peptide in *Medicago*
769 *truncatula*. Proc Natl Acad Sci USA 114:6848–6853.
770 81. Kazmierczak T, Nagymihály M, Lamouche F, Barrière Q, Guefrachi I, Alunni B, Ouadghiri M,
771 Ibijbijen J, Kondorosi É, Mergaert P, Gruber V. 2017. Specific host-responsive associations
772 between *Medicago truncatula* accessions and *Sinorhizobium* strains. Mol Plant-Microbe Interact
773 30:399–409.
774 82. Gully D, Gargani D, Bonaldi K, Grangeteau C, Chaintreuil C, Fardoux J, Nguyen P, Marchetti R,
775 Nouwen N, Molinaro A, Mergaert P, Giraud E. 2016. A peptidoglycan-remodeling enzyme is
776 critical for bacteroid differentiation in *Bradyrhizobium* spp. during legume symbiosis. Mol Plant-
777 Microbe Interact 29:447–457.
778 83. Khan SR, Gaines J, Roop RM 2nd, Farrand SK. 2008. Broad-host-range expression vectors with
779 tightly regulated promoters and their use to examine the influence of TraR and TraM expression
780 on Ti plasmid quorum sensing. Appl Environ Microbiol 74:5053-5062.
781 84. Ducret A, Quardokus EM, Brun YV. 2016. MicrobeJ, a tool for high throughput bacterial cell
782 detection and quantitative analysis. Nat Microbiol 1:16077.
783 85. Schneider CA, Rasband WS, Eliceiri KW. 2012. NIH Image to ImageJ: 25 years of image analysis.
784 Nat Methods 9:671–675.
785 86. Benincasa M, Barrière Q, Runti G, Pierre O, Bourge M, Scocchi M, Mergaert P. 2016. Single Cell
786 Flow Cytometry Assay for Peptide Uptake by Bacteria. Bio-protocol 6:e2038–e2038.
787

788 **Figures and legends**

789

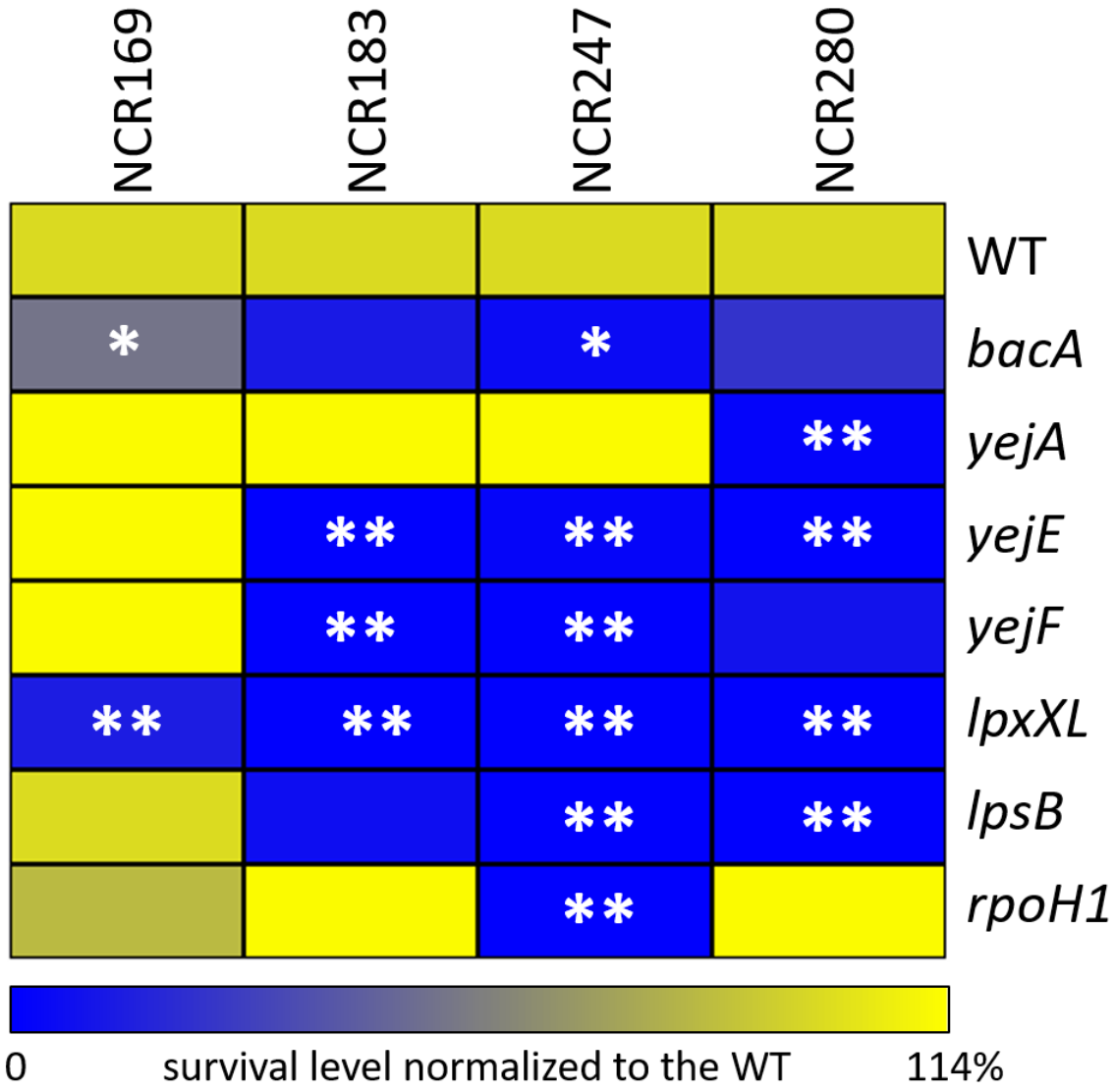

790

791 **Figure 1. Sensitivity profile of *Sinorhizobium meliloti* strains to a panel of NCR peptides.** The
792 heatmap shows the relative survival, expressed in % of the mutant strains compared to the wild type
793 (WT) survival set at 100% for each peptide treatment. Nonparametric Kruskal-Wallis and post-hoc
794 Dunn tests were used to assess the significance of differences which are indicated by asterisks (** is
795 $p<0.05$; * is $p<0.1$). One representative experiment out of two is shown.

796

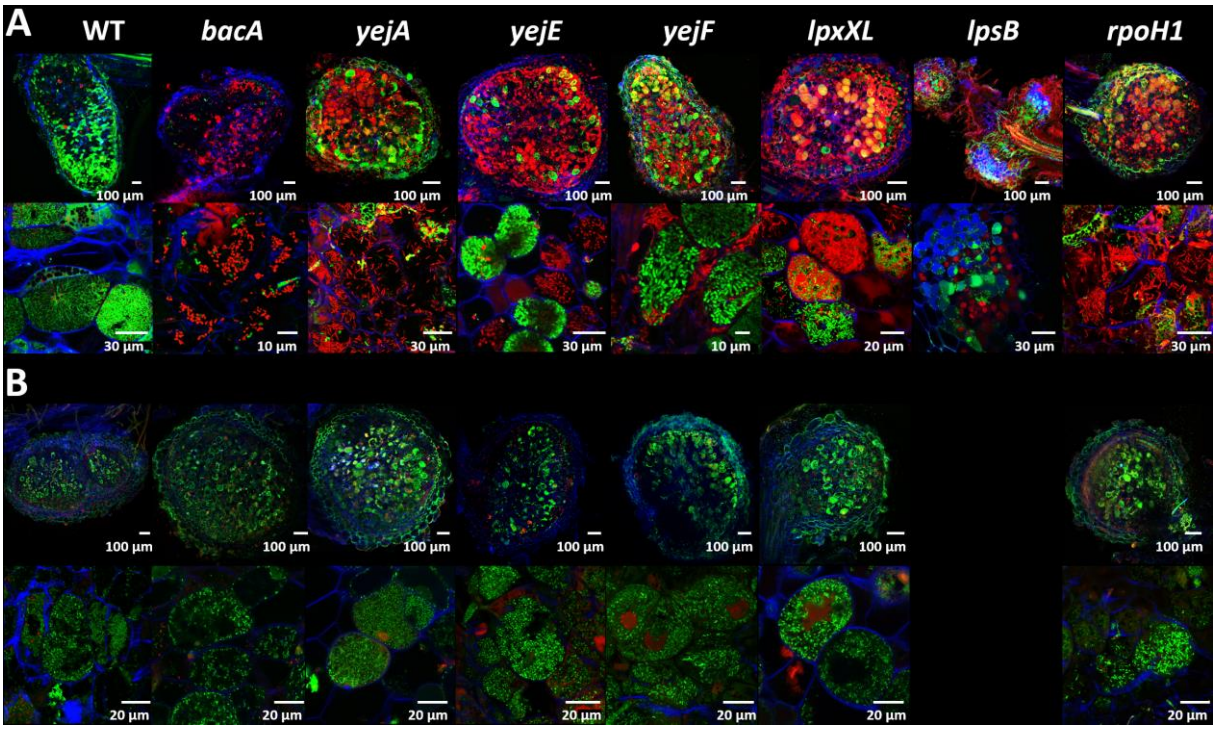

Figure 2. Symbiotic phenotype of *Sinorhizobium meliloti* mutants during symbiosis with *Medicago truncatula* wild type and *dnf1* mutant. A. Membrane permeability in bacteroids of *S. meliloti* Sm1021 wild type (WT) and mutants in wild-type *M. truncatula* nodules, determined by live-dead staining of nodule sections and confocal microscopy. **B.** Membrane permeability of *S. meliloti* Sm1021 WT and mutants in nodules of the *M. truncatula dnf1* mutant, determined by live-dead staining of nodule sections and confocal microscopy. Nodule phenotype at 21 days post inoculation. Top row images, full nodule sections; Bottom row images, enlarged images of symbiotic cells. Scale bars are indicated in each panel. The staining procedure of nodule sections with a mixture of the dyes propidium iodide, SYTO™9 and calcofluor-white highlights the bacteroids and nodule bacteria with a green fluorescence signal (SYTO™9) when their membranes are well preserved and with a red fluorescence (propidium iodide) when their membranes are highly permeable. Plant cell walls are stained blue (calcofluor-white). Representative images are shown out of five to 10 nodules analyzed per condition and originating from at least two independent nodulation assays.

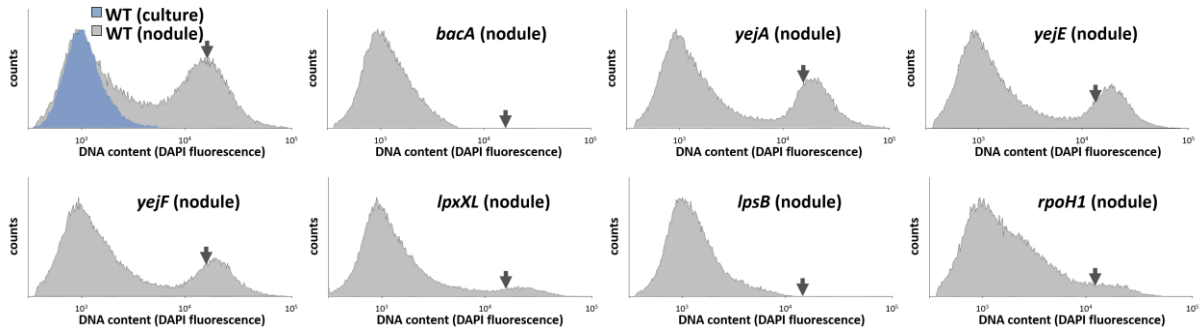

Figure 3. DNA content of nodule bacteria in *Medicago truncatula*. Flow cytometry analysis of the DNA content of bacteria in culture or isolated from nodules infected with the indicated strains and stained with 4',6-diamidino-2-phenylindole (DAPI). The cell counts (y-axes) are represented in function of the DAPI fluorescence intensity (x-axes). The arrow in each graph indicates the mean DNA content of wild-type (WT) bacteroids as in the upper left panel. One representative experiment out of two is shown.

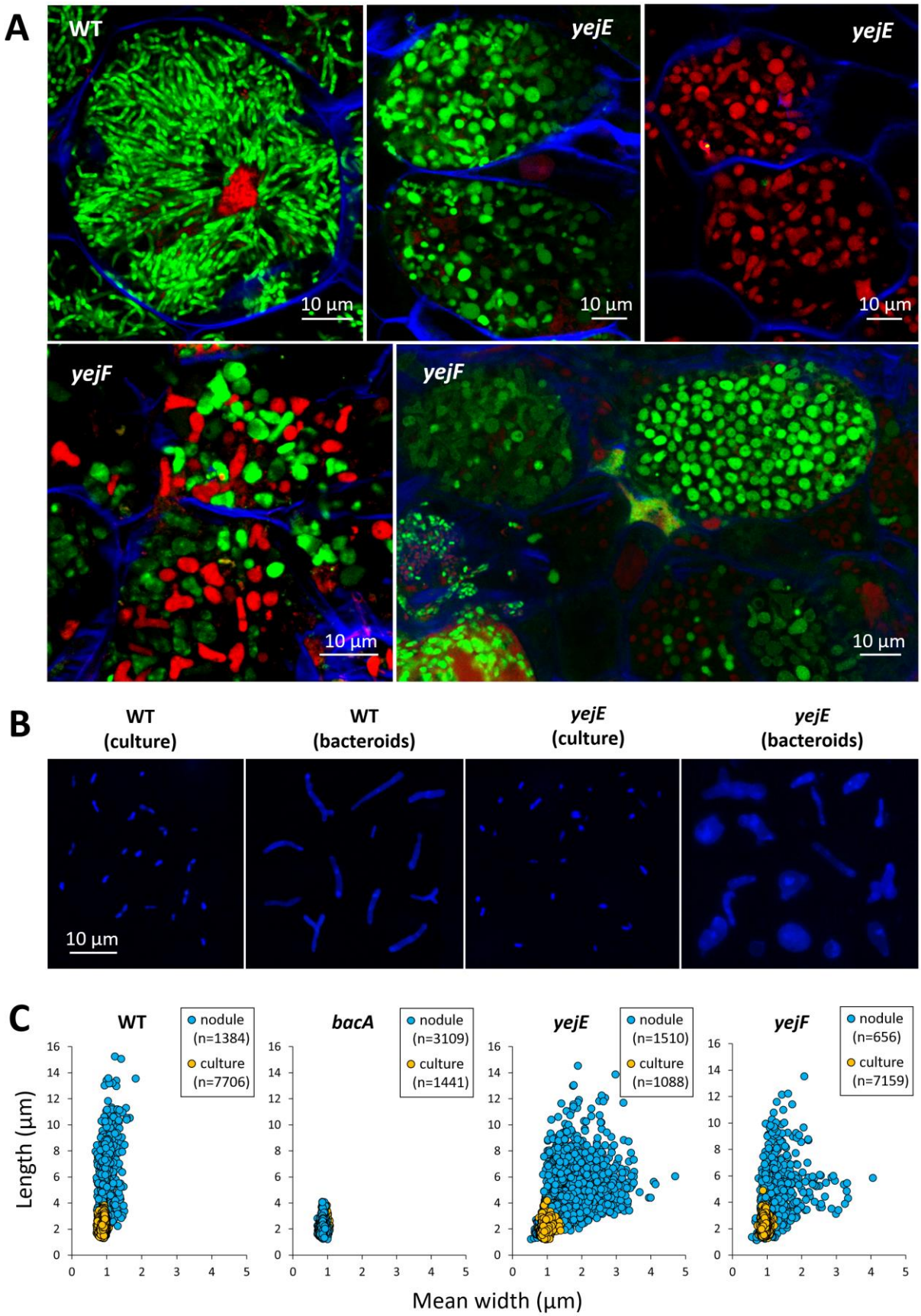

Figure 4. Bacteroid morphology of *yejE* and *yejF* mutants in *Medicago sativa* nodules. A. Sections of nodules infected with the wild type (WT) and the *yejE* or *yejF* mutants were stained with a mixture of the dyes propidium iodide, SYTO™9 and calcofluor-white and observed by confocal microscopy.

824 Scale bars (10 µm) are indicated in each panel. Representative images are shown out of five to 10
825 nodules analyzed per condition and originating from at least two independent nodulation assays. **B.**
826 Preparations of cultured bacteria or purified *M. sativa* nodule bacteria of the wild type and the *yejF*
827 mutant were observed by fluorescence microscopy. The panels are composite images and the shown
828 individual cells were cut from original images and recombined in a single panel. Each panel is at the
829 same magnification and the scale bar (10 µm) is indicated in the left panel. **C.** Cell shape parameters
830 of free-living bacteria and bacteroids determined by MicrobeJ. Dot plots show the mean width and
831 length of cells of the indicated strains. Each point represents the values of one bacterium. Numbers
832 of analysed cells (n) are indicated.
833

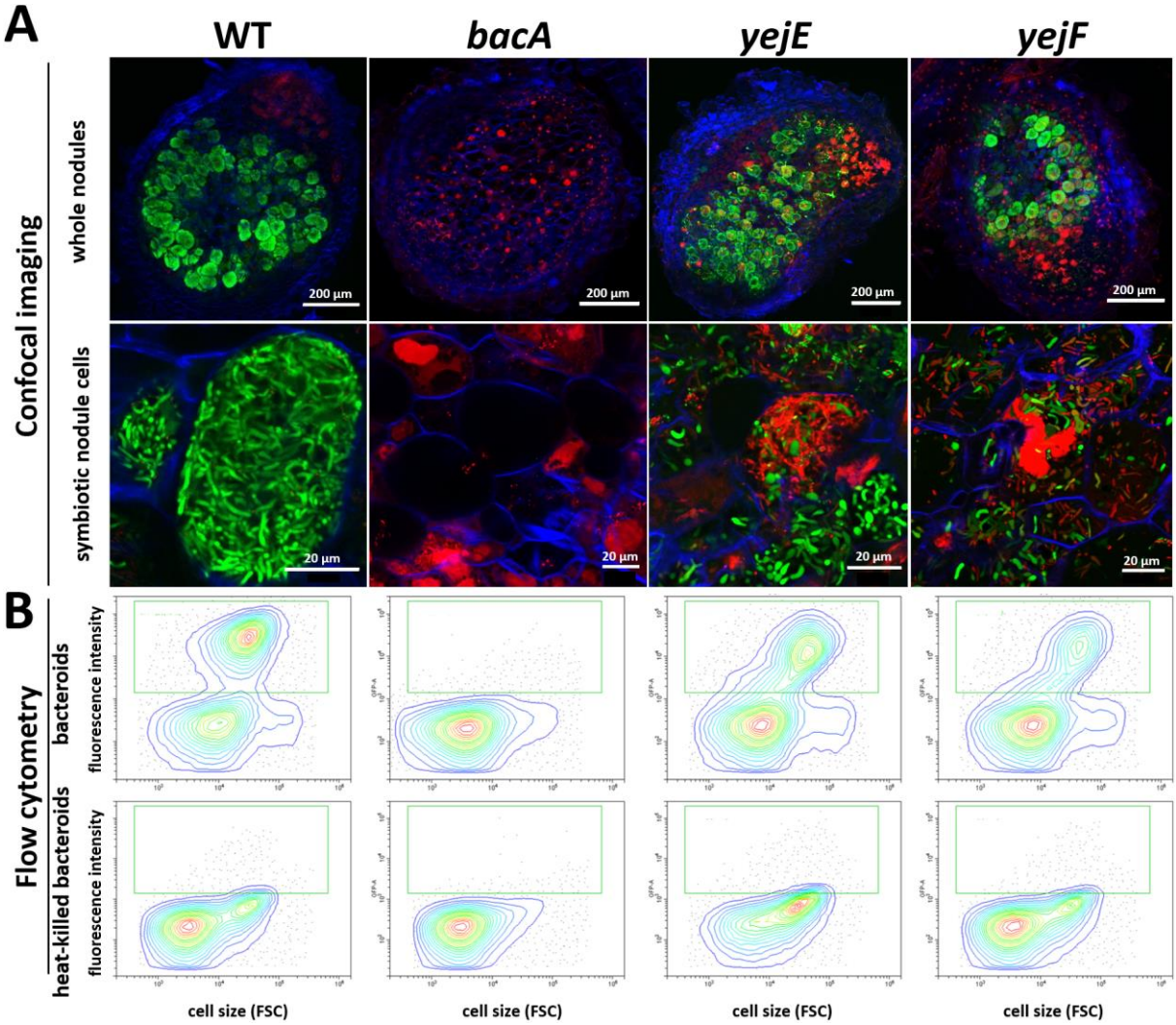

Figure 5. Nitrogenase expression in the *yejE* and *yejF* mutant bacteroids in *Medicago truncatula* nodules. A. Confocal microscopy of sections of nodules infected with *S. meliloti* Sm1021.p*pnifH-GFP* (WT), *bacA*.p*pnifH-GFP* (*bacA*), *yejE*.p*pnifH-GFP* (*yejE*) or *yejF*.p*pnifH-GFP* (*yejF*) and stained with propidium iodide (red stain). Green stained bacteroids are functional while red stained bacteroids are non-functional. **B.** Flow cytometry determination of GFP levels in nodule bacteria (upper panels) and heat-killed nodule bacteria (lower panels). The green square shows the position of the GFP-positive bacteroids. FSC is forward scatter.

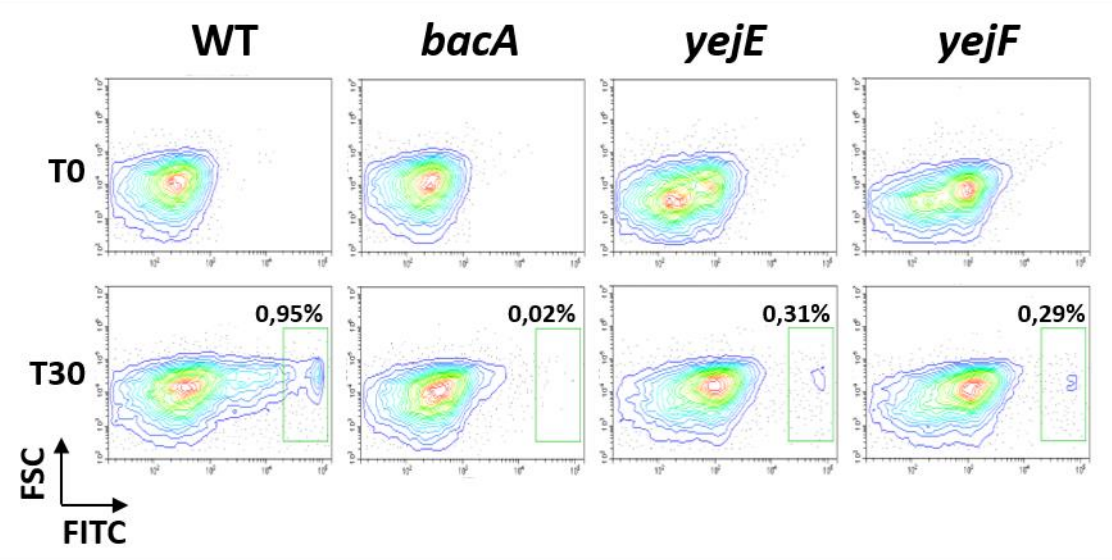

843
844 **Figure 6. Uptake of NCR247 mediated by the BacA and YejABEF transporters.** Flow cytometry
845 measurement of FITC fluorescence in *S. meliloti* cells before (T0) and after 30 minutes of incubation
846 (T30) of the bacteria with the NCR247-FITC peptide. FITC in the x-axis is FITC-derived fluorescence
847 and FSC in the y-axis is forward scatter. The green square shows the bacteria that are FITC-positive
848 and have uptaken the NCR247-FITC peptide. In the wild type (WT), a subpopulation of the bacteria
849 import the NCR247-FITC peptide and in the *bacA* mutant, this population is absent. In the *yejE* and
850 *yejF* mutants, the FITC-positive subpopulation is strongly reduced compared to wild type. The
851 analysis was performed in quadruplicate and a representative example is shown.
852

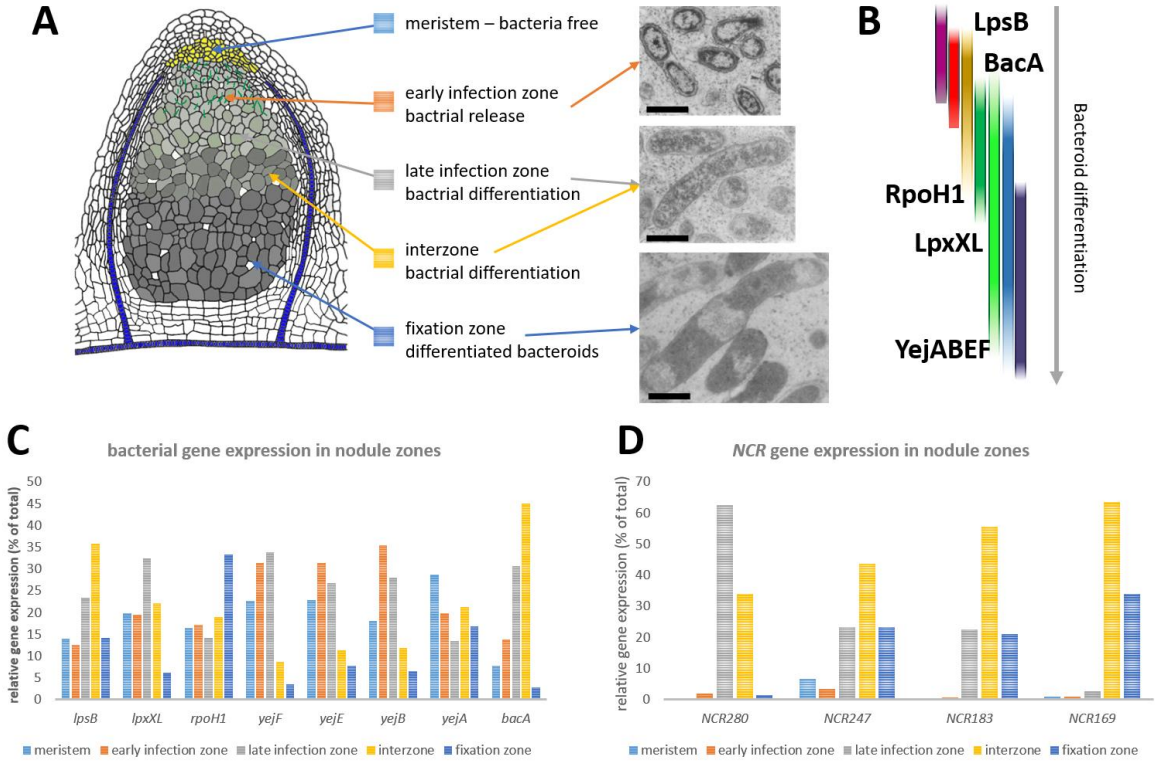

Figure S1. Expression pattern in nodules of bacterial and *NCR* genes. A. Schematic drawing of a *Medicago* nodule organized in functional zones. The meristem is bacteria-free and contains dividing cells allowing the organ to grow. In the early infection zone, bacteria proliferate in infection threads (green lines) and are released by endocytosis inside cells derived from the meristem. In the late infection zone and the so-called interzone, the bacteria differentiate into bacteroids. The fixation zone contains the fully differentiated, nitrogen-fixing bacteroids. The pictures show bacteria inside the nodule cells and are presented at the same scale (bar is 1 µm) allowing to appreciate the transformation of the bacteria. **B.** Against the backdrop of a changing landscape of NCR peptides (rainbow colors representing schematically peptides appearing and disappearing at different stages of symbiotic cell differentiation), the bacterial functions described in this study are critical at distinct stages of the bacteroid differentiation process. It should be noted that the functions that are essential in early stages, such as LpsB and BacA, can also be important in later stages of the bacteroid differentiation. However, the phenotypic analysis of the corresponding mutants cannot reveal these putative late roles. **C,D.** The relative expression profile (% of total) of the studied bacterial genes *lpsB*, *lpxXL*, *rpoH1*, *yejF*, *yejE*, *yejB*, *yejA* and *bacA* (**C**) and of *NCR280*, *NCR247*, *NCR183* and *NCR169* (**D**) in the meristem, early infection zone, late infection zone, interzone and fixation zone are displayed. Data was extracted from (15) and was obtained by RNA-seq analysis on laser-microdissected nodule tissues (33).

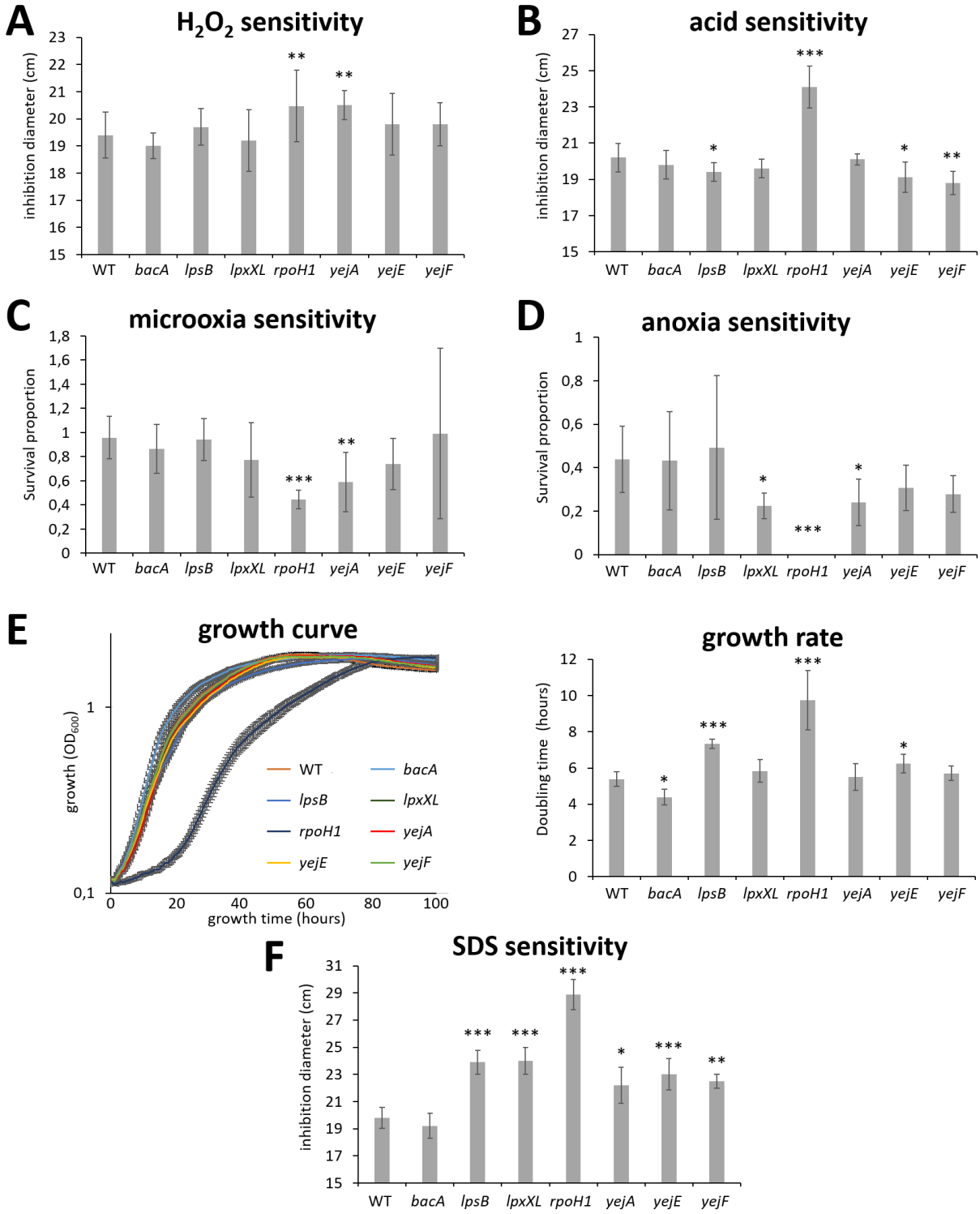

Figure S2. Phenotypes of *Sinorhizobium meliloti* mutants in *in vitro* stress conditions. A. Growth inhibition in the presence of H_2O_2 (n=10). **B.** Growth inhibition in the presence of HCl (n=10). **C.** Growth inhibition in microoxia (n=4). **D.** Growth inhibition in anoxia (n=4). **E.** Growth curves and growth rate in liquid medium (n=10). **F.** Growth inhibition in the presence of SDS (n=10). Growth inhibition in (**A**,**B**,**F**) was determined by the size of a halo formed around a paper patch soaked in the stress compound and in (**C**,**D**) by colony forming units counting. Error bars in all panels are standard deviations. Nonparametric Kruskal-Wallis and post-hoc Dunn tests were used to assess the

881 significance of differences in the data of panels A to F (* is $p<0.05$; ** is $p<0.01$; *** is $p<0.001$). One
882 representative experiment out of at least two is shown.
883

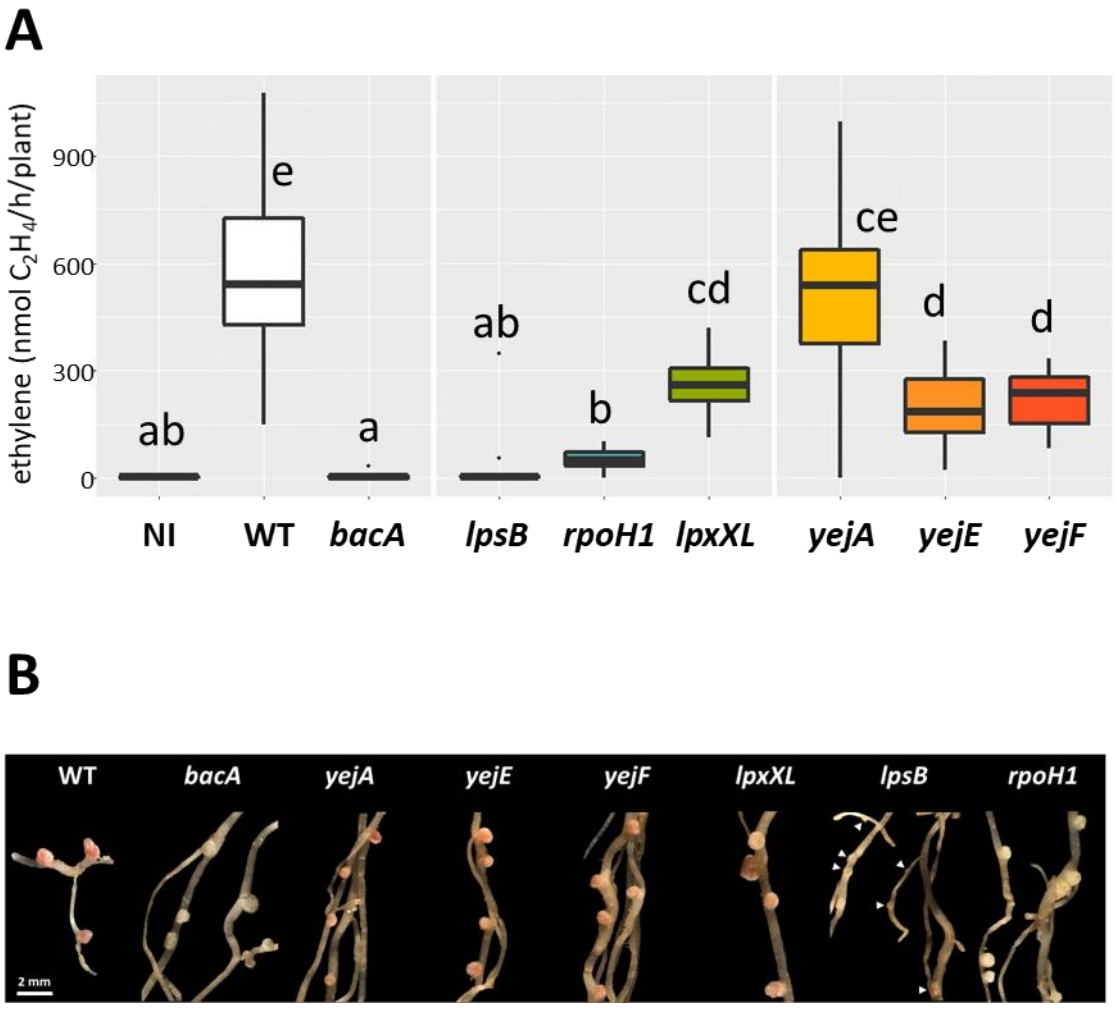

Figure S3. Symbiotic phenotypes of *Sinorhizobium meliloti* NCR-sensitive mutants in *Medicago truncatula*. A. Nitrogen fixation activity determined by the acetylene reduction assay on whole roots of nodulated plants infected with the indicated bacterial mutants at 21 days post inoculation. NI, non-inoculated control plants; WT, plants nodulated by the wild-type strain Sm1021. Boxplots were generated from 15 plants each. Letters associated with each condition represent statistically different classes determined by a non-parametric Dunn test, with a α threshold equal to 0.05. **B.** Nodule phenotypes at 21 days post inoculation. Arrowheads indicate small nodules elicited by the *lpsB* mutant. Scale bar (2 mm) applies to all panels.

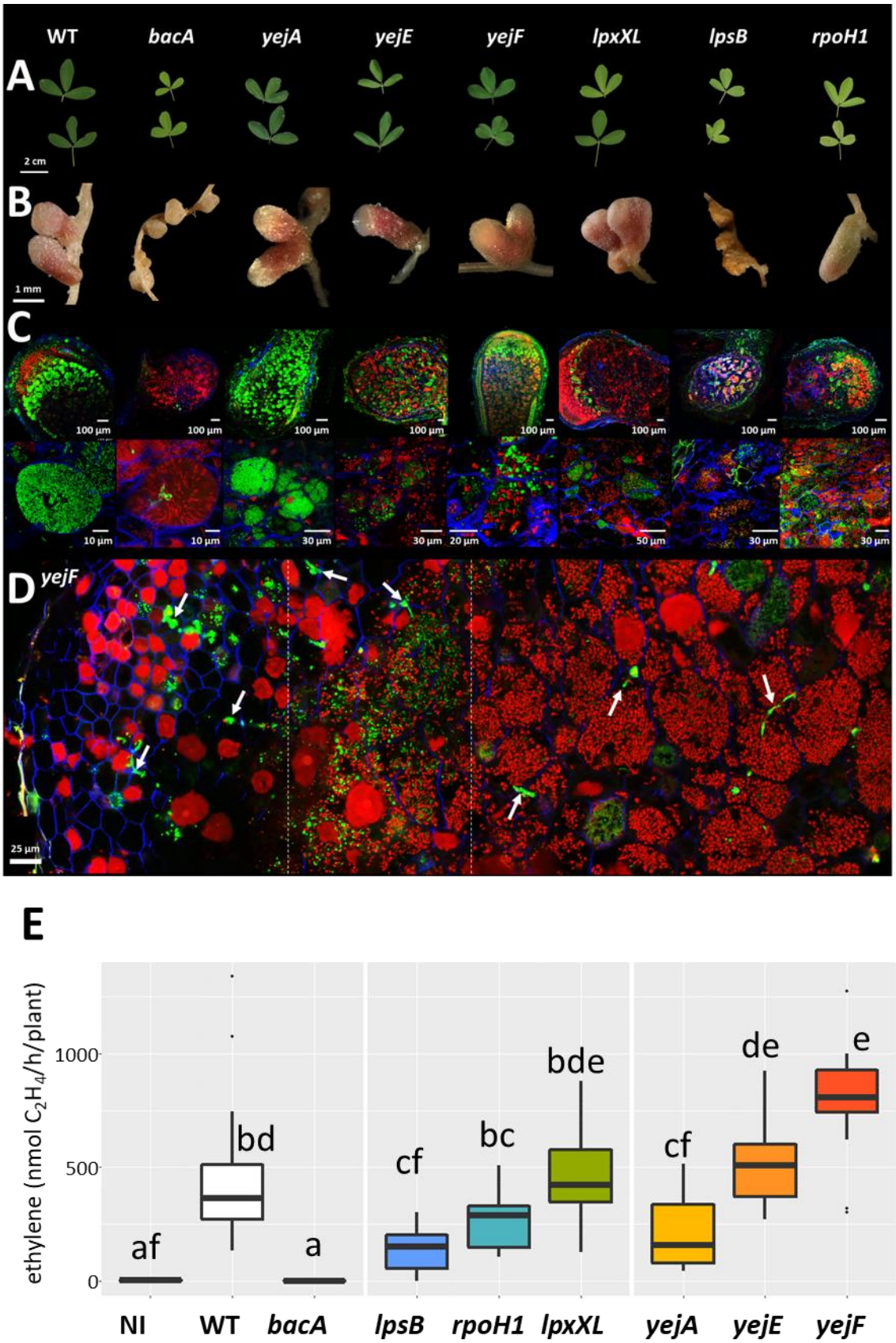

894
895 **Figure S4. Symbiotic phenotype of *Sinorhizobium meliloti* mutants during symbiosis with *Medicago***
896 ***sativa*. A.** Leaves of plants inoculated with the indicated bacterial strains. Scale bar = 2 cm. **B.** Nodule
897 phenotype at 21 days post inoculation. Scale bar = 1 mm. **C.** Bacteroid viability determined by live-

898 dead staining of nodule sections and confocal microscopy. Top row images, full nodule sections;
899 Bottom row images, enlarged images of symbiotic cells. Scale bars are indicated in each panel. **D.**
900 Composite image of a *yejF*-infected nodule section showing the rapid permeabilization of the
901 membranes of the internalized bacteria (red staining). Note the bacteria in infection threads (white
902 arrows) are not permeabilized (green staining). The images of the composition are separated by
903 dashed lines. **E.** Nitrogen fixation activity determined by the acetylene reduction assay on whole
904 roots of nodulated plants infected with the indicated bacterial mutants at 21 days post inoculation.
905 NI, non-inoculated control plants; WT, plants nodulated by the wild-type strain Sm1021. Boxplots
906 were generated from 15 plants each. Letters associated with each condition represent statistically
907 different classes determined by a non-parametric Dunn test, with a α threshold equal to 0.05.
908

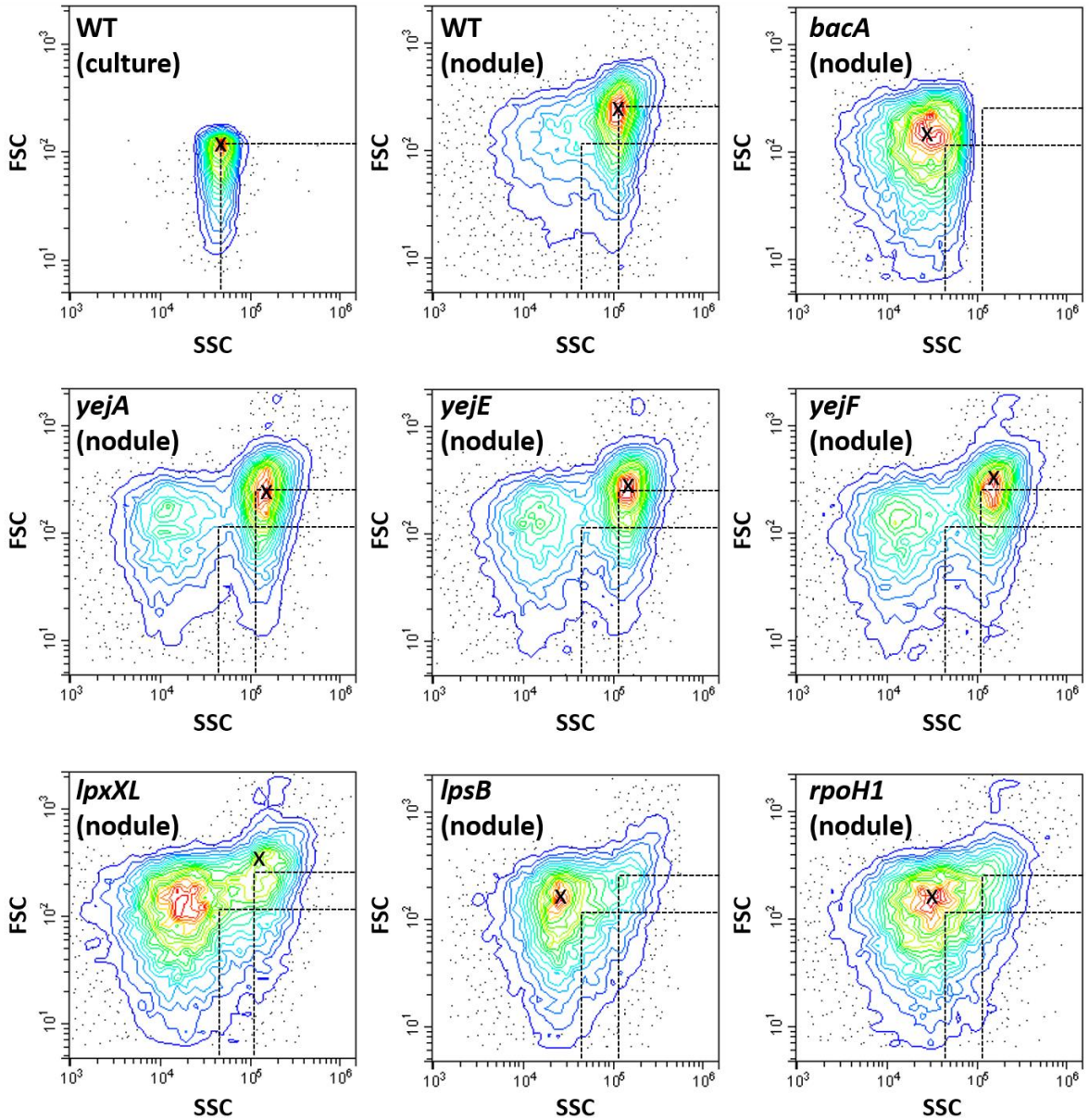

Figure S5. Morphological parameters in nodule bacteria of *Medicago truncatula* nodules. Flow cytometry analysis of the morphology of bacteria isolated from nodules infected with the indicated strains. The forward scatter (FSC, y-axes) is represented in function of the side scatter (SSC, x-axes). The "X" indicates the peak values for each sample. The position of the peak value in the cultured bacteria and in the wild-type bacteroids are indicated in each panel by the hatched lines.

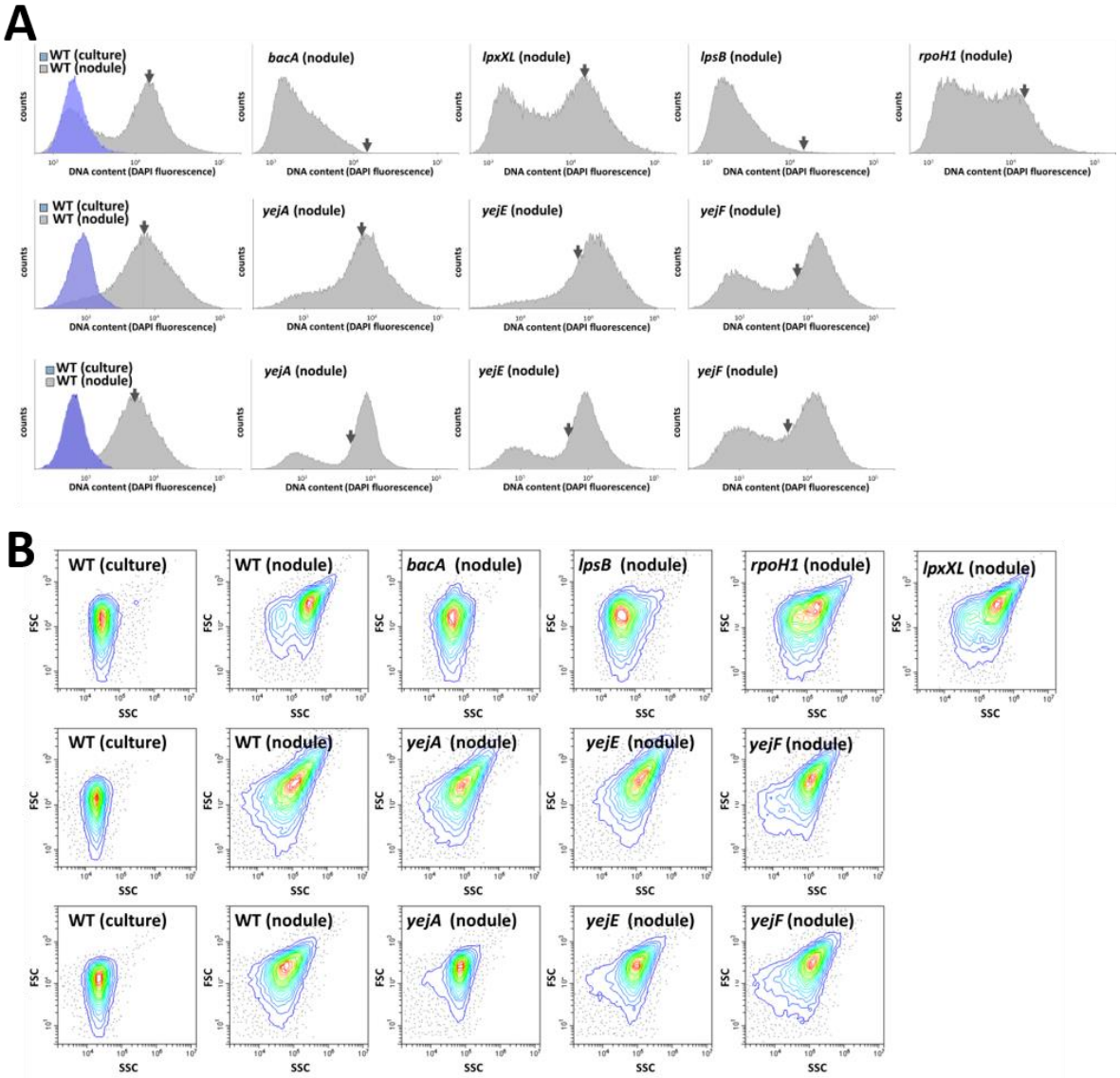

Figure S6. DNA content and morphological parameters in nodule bacteria in *Medicago sativa*. A. Flow cytometry analysis of the DNA content of bacteria in culture or isolated from nodules infected with the indicated strains and stained with 4',6-diamidino-2-phenylindole (DAPI). The cell counts (y-axes) are represented in function of the DAPI fluorescence (x-axes). The arrow in each panel indicates the mean DNA content of wild-type bacteroids. The rows represent three sets of independent experiments and the values of DAPI fluorescence cannot be compared between experiments because of differences in instrument settings. The first two rows are samples prepared from 21 dpi nodules; the third row is from 32 dpi nodules. The latter shows that the phenotype of the *yejA* mutant evolves in older nodules. **B.** Flow cytometry analysis of the morphology of bacteria isolated from nodules infected with the indicated strains. The forward scatter (FSC, y-axes) is represented in function of the side scatter (SSC, x-axes).

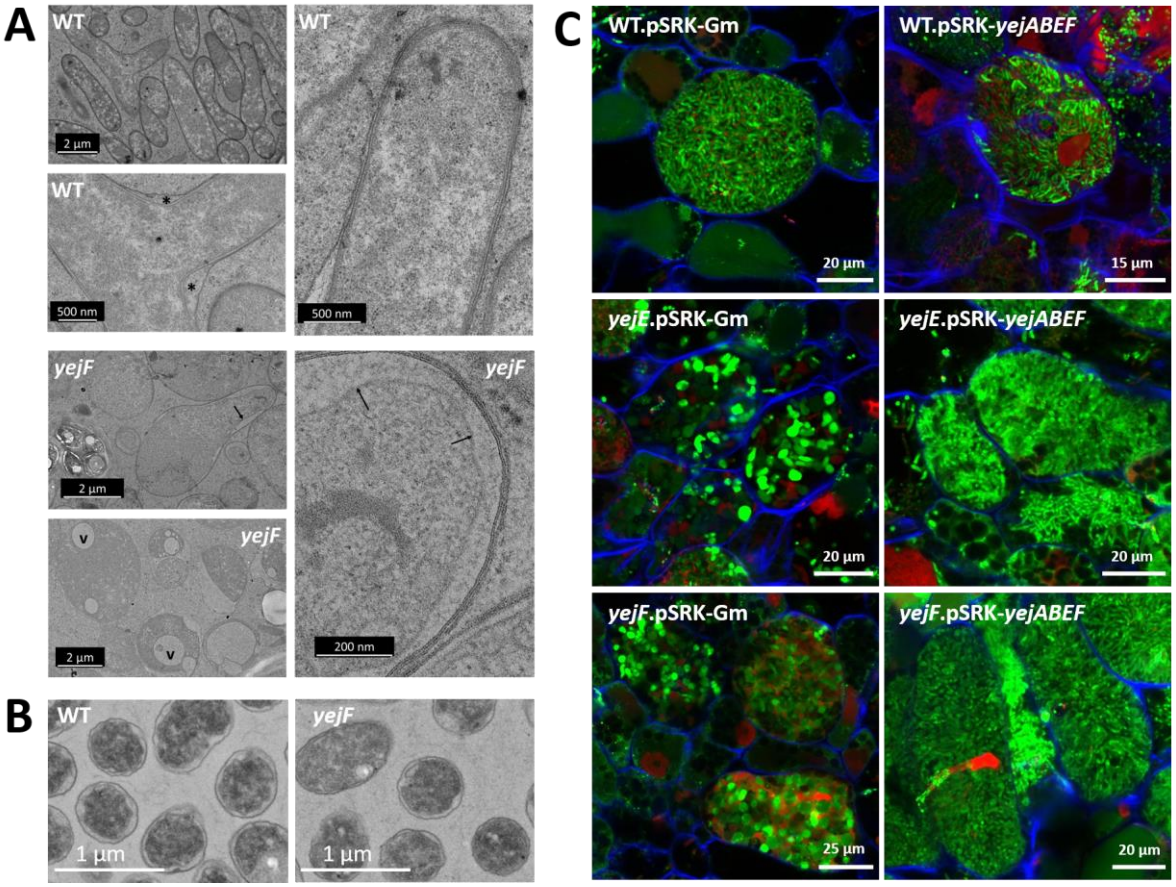

929
930 **Figure S7. Cellular defects in the *yejF* mutant bacteroids in *Medicago sativa* nodules. A.**
931 Transmission electron microscopy of wild type (WT) and *yejF* mutant bacteroids. The arrows indicate
932 retracted inner membranes in the *yejF* bacteroids, "v" indicate vacuoles and "*" indicate an enlarged
933 peribacteroid space found in the angle of a branched bacteroid. **B.** Ultrastructure of wild type (WT)
934 and the *yejF* mutant bacteria in culture by transmission electron microscopy. Scale bars are 1 µm. **C.**
935 Confocal microscopy of sections of nodules infected with wild type (WT), *yejE* or *yejF* mutant bacteria
936 carrying the empty plasmid pSRK-Gm or the complementing plasmid pSRK-*yejABEF*.
937

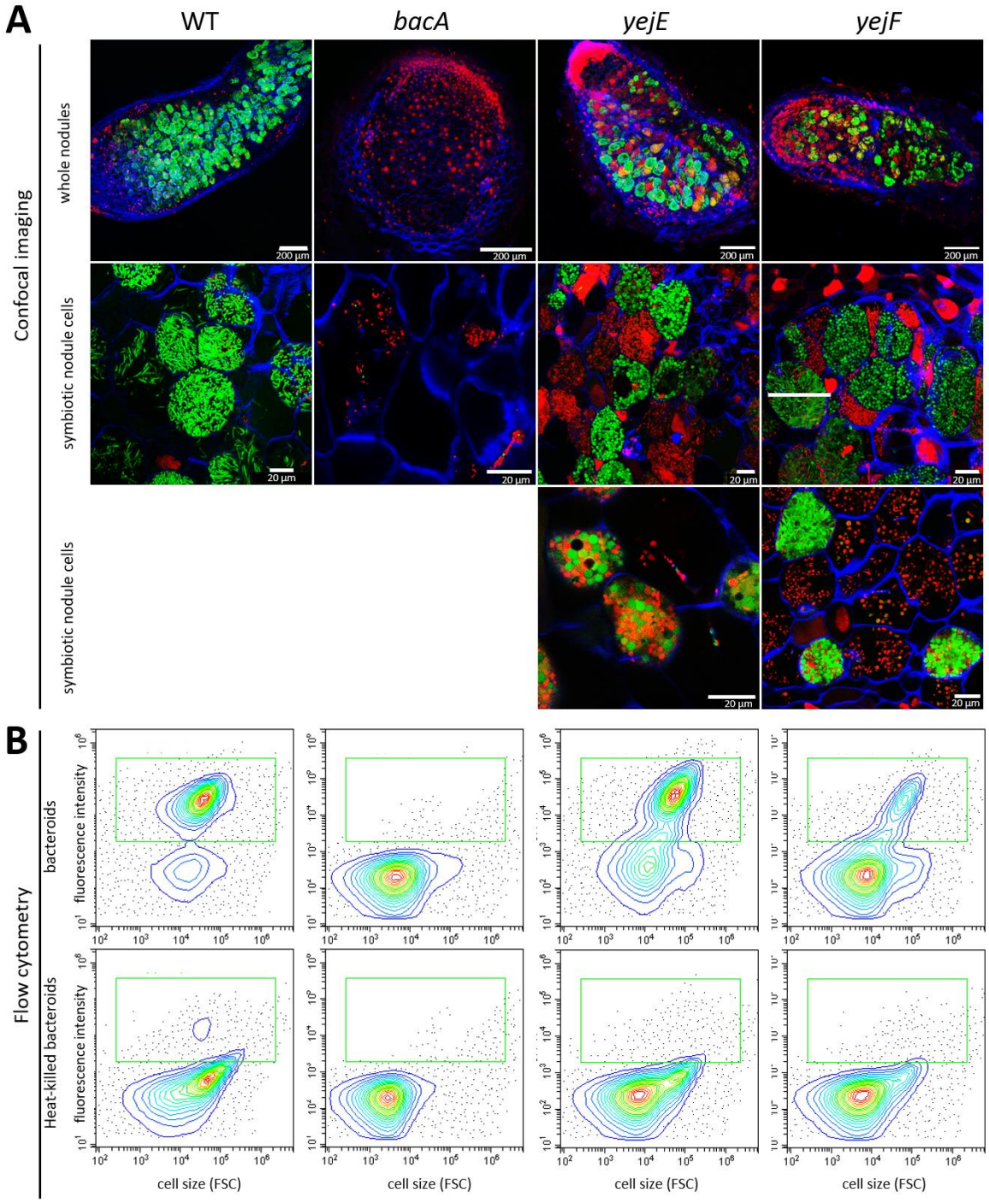

Figure S8. Nitrogenase expression in the *yejE* and *yejF* mutant bacteroids in *Medicago sativa* nodules. A. Confocal microscopy of sections of nodules infected with *S. meliloti* Sm1021.p*pnifH-GFP*, *bacA*.p*pnifH-GFP*, *yejE*.p*pnifH-GFP* or *yejF*.p*pnifH-GFP* and stained with propidium iodide (red stain). Green stained bacteroids are functional while red stained bacteroids are non-functional. **B.** Flow cytometry determination of GFP levels in nodule bacteria (upper panels) and heat-killed nodule bacteria (lower panels). The green square shows the position of the GFP-positive bacteroids. FSC is forward scatter.

peptide (concentration)	survival (%) relative to untreated bacteria (n=3)	Standard deviation	survival relative to WT (%)	*p* -value (Dunn test)
NCR169 (10 µM)				
WT	8,73	3,41	100,00	
bacA	4,80	4,43	55,00	0,05
yejA	10,91	8,52	125,00	0,30
yejE	9,45	1,70	108,33	0,26
yejF	13,67	8,86	156,67	0,23
lpxXL	1,02	0,34	11,67	0,02
lpsB	6,55	1,70	75,00	0,48
rpoH	7,56	0,68	86,67	0,23
NCR183 (10 µM)				
WT	0,05	0,03	100,00	
bacA	0,01	0,01	12,50	0,24
yejA	0,13	0,11	275,00	0,27
yejE	0,00	0,00	0,00	0,02
yejF	0,00	0,00	0,00	0,02
lpxXL	0,00	0,00	0,00	0,02
lpsB	0,00	0,01	5,00	0,12
rpoH	0,23	0,15	487,50	0,15
NCR247 (25 µM)				
WT	0,03	0,02	100,00	
bacA	0,00	0,00	3,85	0,08
yejA	0,05	0,00	153,85	0,37
yejE	0,00	0,00	3,85	0,03
yejF	0,00	0,00	0,00	0,01
lpxXL	0,00	0,00	0,00	0,01
lpsB	0,00	0,00	0,00	0,01
rpoH	0,00	0,00	0,00	0,01
NCR280 (25 µM)				
WT	0,05	0,01	100,00	
bacA	0,01	0,02	23,91	0,23
yejA	0,00	0,00	2,17	0,02
yejE	0,00	0,00	0,00	0,01
yejF	0,01	0,01	10,87	0,14
lpxXL	0,00	0,00	0,00	0,01
lpsB	0,00	0,00	0,00	0,01
rpoH	0,07	0,02	134,78	0,29
NCR247 (25 µM)				
WT.pSRK-Gm	0,16	0,04	100,00	
yejF .pSRK-Gm	0,00	0,00	0,12	0,01
WT.pSRK-*yejABEF*	0,14	0,04	87,99	0,36
yejF .pSRK-*yejABEF*	0,19	0,08	117,20	0,36

Table S1. Survival after NCR treatment of wild-type and mutant *Sinorhizobium meliloti*.

	Gene	Primer name	Sequence	Description
Insertion mutants	SMc02829 (*yejF*)	2829forward	CAAATCGGTGTCGACCAACTCGATCCTGAAGCTC	Primers used to amplify a region of *SMc02829* CDS, flanked with SalI & XbaI sites
		2829reverse	GTTGGCTCTAGACATGGCTATCATTAC	
		2829out-f	CATCTCCTTCGACATCAAG	Primers used for verification
		2829out-r	CTCGTCGGCGATCAGGAGCTC	
	SMc02830 (*yejE*)	2830forward	CTTCGGCCTGTCGACGTTTGCCGAGTTCATC	Primers used to amplify a region of *SMc02830* CDS, flanked with SalI & XbaI sites
		2830reverse	CAGCGCTCTAGAGAAAAGGACCGAGATG	
		2830out-f	CTGGCTCTTCCTCCTCCTCTTC	Primers used for verification
		2830out-r	GATGATGAGCAGGATGTAGAG	
	SMc02832 (*yejA*)	2832forward	GCTACGTCGACGATCGGAGAACCCAAATAC	Primers used to amplify a region of *SMc02832* CDS, flanked with SalI & XbaI sites
		2832reverse	GTGACTCTAGACTCGCCTGTCTTTTC	
		2832out-f	CAATGCCGAGGAACAACC	Primers used for verification
		2832out-r	GAGAATGTTCGGCAGTTC	
	SMc00646 (*rpoH1*)	RpoH1-Sal1-forward	CGCACAGTCGACTAACGAGCCATCTTCGCCTC	Primers used to amplify a region of *SMc00646* CDS, flanked with SalI & XbaI sites
		RpoH1-Xba1-Reverse	CGAAGATCTAGAGCTCACGATCGTTCAGAACC	
		RpoH1-up	AAGCGGTATCAGGAG	Primers used for verification
		RpoH1-down	CCTCCTGCACCTTTT	
Deletion mutants	SMc02829 (*yejF*)	2829fup	GCAACGGCACCATCATGGATCCGCACC	Up fragment used for deletion of *SMc02829*
		2829rup	GGAGAAACTCGGAACGTCTTTCTCG	
		2829fdown	CGTTCCGAGTTTCTCCCATGC	Down fragment used for deletion of *SMc02829*
		2829rdown	CACCCACTCGCTCATCCAAGCTTTCAGG	
	SMc02830 (*yejE*)	2830fup	GGACACGTGTTCCGCAACGGATCCCTGATC	Up fragment used for deletion of *SMc02830*
		2830rup	CGTCGCGCCAGACGTCCCTCCG	
		2830fdown	GGACGTCTGGCGCGACGATGACAG	Down fragment used for deletion of *SMc02830*
		2830rdown	GCGAACATGCCTGAAAGCTTCGTCG	
	SMc02832 (*yejA*)	2832fup	GGTCGAACCGCAGGGATCCAGCGCAGCACG	Up fragment used for deletion of *SMc02832*
		2832rup	GCAAGAGCTCCGGCCGGTACCCC	
		2832fdown	CGGCCGGAGCTCTTGCGCTCAGG	Down fragment used for deletion of *SMc02832*
		2832rdown	CATGATGCCGACGATCGTCAAGCTTATCAGC	
comple-mentation	*yejABEF*	yejA_NdeI_F	ATTATAATCATATGCCAAACTTCTGCAGGACCG	upstream primer for cloning of yejABEF in pSRK(Gm)
		yejF_XbaI_R	ATAATTATCTAGACTACTGATGAACGGCGGC	downstream primer for cloning of yejABEF in pSRK(Gm)
		LacI_F	ACGACAGGTTTCCCGACTGG	primer for construct verification in pSRK(Gm)
		T7_F	TAATACGACTCACTATAGGG	primer for construct verification in pSRK(Gm)

Table S2. Primers used for mutant constructions.